HHS Public Access

Author manuscript

Cancer Cell. Author manuscript; available in PMC 2019 January 08.

Published in final edited form as:

Cancer Cell. 2018 January 08; 33(1): 108–124.e5. doi:10.1016/j.ccell.2017.12.001.

Hedgehog pathway drives fusion-negative rhabdomyosarcoma initiated from non-myogenic endothelial progenitors

Catherine J. Drummond[1,4], **Jason A. Hanna**[1,4], **Matthew R. Garcia**[1], **Daniel J. Devine**[1], **Alana J. Heyrana**[1], **David Finkelstein**[2], **Jerold E. Rehg**[3], and **Mark E. Hatley**[1,5,*]

[1]Department of Oncology, St. Jude Children's Research Hospital, 262 Danny Thomas Place, Memphis, TN 38105, USA

[2]Department of Computational Biology, St. Jude Children's Research Hospital, 262 Danny Thomas Place, Memphis, TN 38105, USA

[3]Department of Pathology, St. Jude Children's Research Hospital, 262 Danny Thomas Place, Memphis, TN 38105, USA

SUMMARY

Rhabdomyosarcoma (RMS) is a pediatric soft tissue sarcoma that histologically resembles embryonic skeletal muscle. RMS occurs throughout the body and an exclusively myogenic origin does not account for RMS occurring in sites devoid of skeletal muscle. We previously described a RMS model activating a conditional constitutively active *Smoothened* mutant (SmoM2) with *aP2-Cre*. Using genetic fate mapping, we show SmoM2 expression in Cre expressing endothelial progenitors results in myogenic transdifferentiation and RMS. We illustrate endothelium and skeletal muscle within the head and neck arise from *Kdr* expressing progenitors and that hedgehog pathway activation results in aberrant expression of myogenic specification factors as a potential mechanism driving rhabdomyosarcomagenesis. These findings suggest that RMS can originate from aberrant development of non-myogenic cells.

Graphical abstract

Using genetic fate mapping, Drummond et al. show that hedgehog pathway activation in endothelial progenitors results in aberrant expression of myogenic specification factors, myogenic transdifferentiation, and rhabdomyosarcoma (RMS). The finding may explain how RMS develops in sites devoid of skeletal muscle.

[*]Address correspondence to: Mark E. Hatley, 262 Danny Thomas Place, Department of Oncology, MS-352, Memphis, TN 38105, Phone: 901-595-7952, mark.hatley@stjude.org.

[4]These authors contributed equally

[5]Lead contact

AUTHOR CONTRIBUTIONS

Conceptualization, C.J.D., J.A.H, D.J.D and M.E.H.; Methodology, C.J.D., J.A.H., M.R.G., D.J.D. and M.E.H.; Formal Analysis, C.J.D., J.A.H., J.E.R. and M.E.H.; Investigation, C.J.D., J.A.H., M.R.G., D.J.D., and A.J.H.; Data Curation, D.F.; Writing-Original Draft, C.J.D and M.E.H.; Writing – Reviewing and Editing, C.J.D. J.A.H., M.R.G, D.J.D, A.J.H, J.E.R, D.F. and M.E.H.; Visualization, C.J.D., J.A.H. and M.E.H.; Supervision M.E.H.; Funding Acquisition M.E.H.

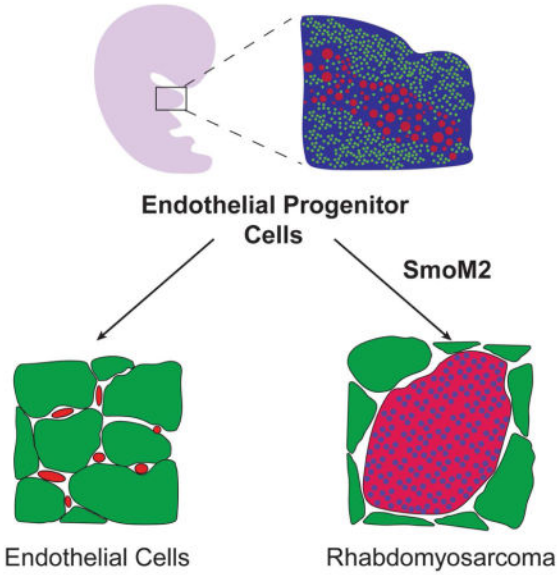

Keywords

Rhabdomyosarcoma; skeletal muscle; endothelium; myogenesis; Tbx1; hedgehog; sarcoma

INTRODUCTION

Rhabdomyosarcoma (RMS) is the most common pediatric soft tissue sarcoma with an incidence of 4.5 cases per million children (Perez et al., 2011). Intensive clinical trials over the past three decades have not improved survival rates or treatment options for high risk patients (Oberlin et al., 2008). RMS is classified into two major histological subtypes, alveolar RMS (ARMS) or embryonal RMS (ERMS) (Parham and Barr, 2013). ARMS tumors typically (~80%) harbor chromosomal translocations resulting in the expression of a PAX3-FOXO1 or PAX7-FOXO1 fusion protein (Davis et al., 1994; Galili et al., 1993) which foretells a worse prognosis. The molecular features and clinical outcomes of ARMS patients lacking *PAX3/PAX7-FOXO1* gene translocations resemble ERMS, thus classifying RMS as either fusion negative (FN-RMS) or fusion positive (FP-RMS) better reflects both the biology and clinical outcomes (Williamson et al., 2010). In addition to tumor histology, pretreatment staging and post-surgical grouping are important prognostic indicators of RMS. Tumor location is a key feature of staging and nearly 40% of all RMS occurs in the head and neck (Sultan et al., 2009). It remains unknown how the cell of origin impacts location and clinical outcome of FN-RMS.

RMS resembles developing skeletal muscle and is hence viewed as an arrested state in normal skeletal muscle development (Kashi et al., 2015). During myogenesis the temporal expression of myogenic regulatory factors (Mrfs) Myogenic Differentiation 1 (MYOD1), MYF5, MRF4 (MYF6) and Myogenin drive differentiation and a terminal cell cycle exit (Buckingham and Rigby, 2014). RMS cells express Mrfs, yet fail to execute terminal muscle differentiation. Thus, RMS is thought to originate in muscle progenitor cells. However, an

exclusively myogenic origin of RMS does not account for FN-RMS occurring in sites devoid of skeletal muscle such as the salivary gland, gallbladder, prostate and bladder suggesting additional non-myogenic origins for FN-RMS.

Muscles in the head and neck are derived from the branchial arches and cranial mesoderm and have distinct embryonic origins from somite derived trunk and limb muscles (Michailovici et al., 2015). The specification of head and neck muscle progenitor cells also differs from the somite. In contrast to the trunk and limbs where PAX3 drives Mrf expression, a combination of transcription factors including TBX1, Musculin, TCF21, ISL1, LHX2, and PITX2 act upstream of Mrfs in the head and neck (Buckingham, 2017). It remains unclear how these differing developmental programs contribute to tumorigenesis in RMS.

The Sonic Hedgehog (Shh) pathway is critically involved in tissue morphogenesis including skeletal muscle but not in the muscle of the head and neck (Borycki et al., 1999; Munsterberg et al., 1995). Hedgehog signaling is maintained inactive by the transmembrane receptor Patched1 (PTCH1) binding and repressing Smoothened (SMO). Upon Shh ligand binding PTCH1, SMO is released from inhibition and activates the Gli family of transcription factors inducing downstream target gene expression (Pak and Segal, 2016). Aberrant Shh signaling drives a number of experimental FN-RMS models (Hahn et al., 1998; Hatley et al., 2012; Lee et al., 2007; Mao et al., 2006). Furthermore, active Shh signaling is observed in a high proportion of sporadic FN-RMS with 53% harboring amplification of 12q13.3 containing *GLI1*, 73% displaying increased GLI1 protein by immunohistochemistry (IHC), and 33% exhibiting loss of chromosome 9q22 containing *PTCH1* (Bridge et al., 2000; Paulson et al., 2011; Pressey et al., 2011; Zibat et al., 2010). Hedgehog signaling controls self-renewal of FN-RMS tumor propagating cells and hedgehog pathway inhibition reduces chemotherapy resistance (Satheesha et al., 2016). Together, these studies highlight a role for Shh activation in FN-RMS pathogenesis.

Previously, we described a highly penetrant mouse model of FN-RMS, *aP2-Cre;Smo*$^{M2/+}$, driven by conditional expression of constitutively active SmoM2 by Cre recombinase expressed from the adipocyte protein 2 (aP2) gene promoter. The histology and gene expression of *aP2-Cre;Smo*$^{M2/+}$ tumors recapitulate both other mouse models and human FN-RMS (Hatley et al., 2012). Interestingly, tumors are anatomically restricted, occurring exclusively in the head and neck. In this study we leverage the *aP2-Cre;Smo*$^{M2/+}$ mouse model to interrogate the cellular origins of FN-RMS.

RESULTS

aP2-Cre labels cells within both adipose tissue and skeletal muscle

The development of FN-RMS from conditional, oncogenic *Smoothened* allele, SmoM2, activation by *aP2-Cre* was surprising. Therefore, we sought to determine the cell of origin of FN-RMS in the *aP2-Cre;Smo*$^{M2/+}$ (AS) mouse model. Previously, *aP2-Cre* (also known as *Fabp4-Cre*) was thought to be adipose restricted, but recent reports indicate a broader tissue expression (Lee et al., 2013; Tang et al., 2008; Urs et al., 2006). First, we bred *Rosa26*$^{mT/mG}$ (mT/mG) reporter mice to *aP2-Cre* mice in the presence and absence of SmoM2 to localize

aP2-Cre expression. The mT/mG reporter expresses membrane-targeted Tomato (mT) in all tissues in the absence of Cre recombinase (Figures S1A&B). After breeding to *aP2-Cre*, the mT-stop cassette is deleted in all cells expressing *aP2-Cre* resulting in the indelible labeling of cells and their progeny with membranous EGFP. We generated *aP2-Cre;mT/mG* and *aP2-Cre;mT/mG;Smo*$^{M2/+}$ mice to explore the role of oncogenic SmoM2 in *aP2-Cre* expressing cells. Consistent with aP2 expression in mature adipose tissue, interscapular brown adipose tissue (BAT), inguinal white adipose tissue (WAT) and perirenal adipose were EGFP positive in both *aP2-Cre;mT/mG* and *aP2-Cre;mT/mG;Smo*$^{M2/+}$ mice (Figures 1A&B and S1C). Discrete EGFP positive cells were also observed within both the kidney and the lung (Figure S1C), reflective of aP2 expression in pulmonary and renal capillary endothelial cells (Elmasri et al., 2009). EGFP expression in the developing sperm indicates *aP2-Cre* expression in the male germline accounting for the high rate of global Cre-mediated recombination observed in offspring from male *aP2-Cre* mice (Figure S1D). No EGFP was observed in the ovary and only 0.4% global reporter activation noted in offspring of female *aP2-Cre* mice. Therefore, we restricted our breeding strategies to exclusively use *aP2-Cre* female mice.

Next, we explored the contribution of *aP2-Cre* labeled cells to skeletal muscle development in the absence or presence of SmoM2. As previously reported, *aP2-Cre* labeled cells surround the myofiber periphery (Lee et al., 2013). We noted this localization was unaffected by SmoM2 expression (Figure 1B). Examination of hindlimb quadriceps femoris (quad) and neck sternocleidomastoid (SCM) skeletal muscles revealed that individual muscle fibers remained *aP2-Cre* negative in both *aP2-Cre;mT/mG* and *aP2-Cre;mT/mG;Smo*$^{M2/+}$ mice. Thus, skeletal muscle did not generally derive from *aP2-Cre* expressing cells irrespective of SmoM2 expression providing further evidence that FN-RMS in our AS model does not originate from myogenic precursors. Since our data is based on the lack of staining, we cannot conclude that skeletal muscle never arises from *aP2-Cre* expressing cells. In contrast, FN-RMS tumors were EGFP positive reflecting tumor cell autonomous Cre-mediated activation of hedgehog signaling driving tumorigenesis. These tumors are invasive with EGFP positive cells infiltrating adjacent normal muscle at the tumor periphery (Figures 1A&C).

Given BAT and skeletal muscle share a common progenitor (Seale et al., 2008) and adipocytes express aP2, we asked whether adipocytes are the origin of tumors in *aP2-Cre;Smo*$^{M2/+}$ (AS) mice. To express SmoM2 in adipocytes we utilized adipose specific *Adipoq-Cre* (Eguchi et al., 2011) and brown adipose specific *Ucp1-Cre* (Kong et al., 2014). However, *Adipoq-Cre;Smo*$^{M2/+}$ or *Ucp1-Cre;Smo*$^{M2/+}$ mutant mice did not develop tumors suggesting mature adipose is not the FN-RMS origin in AS mice (Figures S1E–H). Together, these results demonstrate that oncogenic SmoM2 in *aP2-Cre* expressing cells does not alter adipocytes or skeletal muscle, nor result in skeletal muscle fibers derived from *aP2-Cre* labeled cells.

SmoM2 dependent proliferation of *aP2-Cre* labeled cells during embryogenesis

Next, we focused on determining how SmoM2 expression affects *aP2-Cre* labeled cells in early tumor development. Mice sacrificed as early as P7 had microscopic FN-RMS lesions

on H&E staining (Figure S2A). We thus performed genetic fate mapping of *aP2-Cre* labeled cells in the anterior head and neck during embryonic development in AS mice. We utilized *ROSA26-loxP-stop-loxP-tdTomato* (*R26-tdTom*) reporter mice to compare *aP2-Cre* expressing cells indelibly labeled with the Tomato fluorescent protein in *aP2-Cre;R26-tdTom* (AT) and *aP2-Cre;Smo$^{M2/+}$;R26-tdTom* (AST) mice (Figure S2B). Consistent with the mT/mG fluorescent labeling of FN-RMS (Figure 1C), Tomato and MYOD1 colocalized in tumors from AST mice (Figure S2C). At embryonic day 17.5 (E17.5), regions of BAT in the anterior neck were labeled with Tomato in AT embryos along with scattered cells within skeletal muscle that were clearly distinct from myosin heavy chain (MHC) positive myofibers (Figure 2A). Expression of oncogenic SmoM2 led to expansion of *aP2-Cre* labeled cells between skeletal muscle fibers in AST embryos. Starting at E15.5 the Tomato positive cells were distinctly expanding between MHC positive myofibers at sites where tumors develop in the adult (Figures 2B–E). We confirmed these findings using another independently derived *aP2-Cre* driver, *Fabp4-Cre* (He et al., 2003), to induce the expression of SmoM2. Although *Fabp4-Cre;Smo$^{M2/+}$* mice exhibited perinatal lethality, E16.5 embryos displayed cell expansions between muscle fibers of the head and neck identical to the AS mice (Figure S2D). These data suggest that SmoM2 expression in *aP2-Cre* labeled cells adjacent to the myofibers in the neck results in FN-RMS. Thus, we focused on the *aP2-Cre* labeled cells in the muscle interstitium as a potential origin of FN-RMS in the AS mouse model.

aP2-Cre is not expressed in satellite cells

Activating oncogenes and deleting tumor suppressors in muscle stem cells (satellite cells) results in myogenic sarcomas (Blum et al., 2013; Rubin et al., 2011; Van Mater et al., 2015; Zhang et al., 2015). Although satellite cells constitute a rare population of cells in the myofiber, their localization within muscle is reminiscent of *aP2-Cre* labeled cells that undergo SmoM2 dependent expansion. Thus, we sought to determine whether *aP2-Cre* is expressed during satellite cell specification or following activation and subsequent myogenic differentiation. First, we determined *aP2-Cre* labeled cells within the SCM of adult AT mice were distinct from cells stained with satellite cell marker PAX7 illustrating *aP2-Cre* is not expressed during satellite cell specification (Figures 3A and S3A&B). To determine if *aP2-Cre* is expressed during satellite cell activation and differentiation, we purified satellite cells from *aP2-Cre;R26-LacZ* mice, differentiated cells *in vitro* and performed β-galactosidase staining. Myotubes from *aP2-Cre;R26-LacZ* mice showed no β-galactosidase staining following *in vitro* differentiation in contrast to intense staining observed in differentiated myoblasts transduced with adenovirus expressing Cre recombinase (Figure 3B). Furthermore, *aP2-Cre* labeled cells clearly localized outside the laminin sheath in the interstitium between myofibers in the SCM of AT mice (Figures 3C&D). Thus, satellite cell activation and myogenic differentiation does not induce *aP2-Cre* expression eliminating a satellite cell origin of FN-RMS in the AS model.

aP2-Cre labels endothelial cells in muscle interstitium

Several distinct cell types have been described within the muscle interstitium with some having myogenic potential (Malecova and Puri, 2012). To identify the cell type within the muscle interstitial populations indelibly labeled by *aP2-Cre*, we sorted Tomato positive (Tom

$^{+}$) and negative (Tom^{-}) cells from digested SCM of AT mice (Figures 3E–G). Further confirming that *aP2-Cre* does not label satellite cells, myogenic markers *Pax7* and *Myf5* were exclusively expressed in the Tom^{-} population (Figure 3H). Mature adipose markers *Pparg* and *Ucp1* were not expressed in either Tom^{+} or Tom^{-} cells, suggesting intramuscular adipose was not a large component of AT SCM (Figure 3I). Muscle interstitial cells display distinct gene expression patterns with fibroadipogenic progenitors expressing *Pdgfra* and *Pdgfrb* (Uezumi et al., 2010), mesangioblasts and *Pw1* expressing interstitial cells (PICs) expressing *Pdgfra* and *Peg3 (Pw1)* (Pannerec et al., 2013; Tagliafico et al., 2004), pericytes expressing *Pdgfrb* and *Cspg4 (Ng2)* (Lindahl et al., 1997; Ozerdem et al., 2001), connective tissue fibroblasts expressing *Tcf7l2 (Tcf4)* and *Cspg4* (Mathew et al., 2011) and endothelial cells expressing *Pecam1 (Cd31)*. Of these interstitial cell markers, only *Pecam1* was enriched in the Tom^{+} population (Figure 3J).

To further identify *aP2-Cre* labeled cells, we next used mRNA expression profiling to compare the gene expression profiles of isolated Tom^{+} and Tom^{-} cells with that of cell types found within skeletal muscle. Endothelial specific genes *Pecam1, Cdh5, Kdr, Tek, Gata2* and *Sox18* were significantly enriched in Tom^{+} cells while the myogenic marker *Myf5* and interstitial cell markers *Pdgfra* and *Peg3* were significantly enriched in Tom^{-} cells (Figure S3C). Principle component analysis (PCA) illustrated Tom^{+} cells clustered closely to microvascular endothelial cells (Nolan et al., 2013). In contrast, Tom^{-} cells clustered more closely with satellite cells and PW1^{+} interstitial cells. No similarities were identified between either Tom^{+} or Tom^{-} cells and brown or white adipose (Seale et al., 2007) (Figure 3K). The gene expression profile of Tom^{+} cells was also clearly distinct from recently described *Twist2* expressing interstitial cells (Figure S3D)(Liu et al., 2017). Gene ontology analysis of 489 genes enriched in Tom^{+} cells compared to Tom^{-} cells (Log ratio ≥ 2, $p < 0.05$) revealed genes involved in angiogenesis, endothelial cell migration and vascular development were significantly enriched in the Tom^{+} population (Figure 3L). Altogether, these results suggest that *aP2-Cre* labels endothelial cells within the muscle interstitium. Confirming these findings, Tom^{+} cells express endothelial genes *Tek*, *Cdh5*, *Vwf* and *Kdr* (Figure 3M). As well, *aP2-Cre* labeled cells co-localize with PECAM1 in both cross sections and cultured cells from the SCM of AT mice (Figures 3N&O). Furthermore, *aP2-Cre* labeled cells colocalize with PECAM1 in the anterior neck of E17.5 AT embryos (Figure S3E&F).

Previously, Hettmer et al. defined discrete cell types isolated by FACS from adult *Cdkn2a*$^{-/-}$ mouse skeletal muscle with capacity to form myogenic sarcomas after ectopic expression of Kras^{G12V}. This strategy separates satellite cells (CD45^{-}MAC1^{-}TER119^{-}Sca1^{-}β1-integrin $^{+}$CXCR4^{+}) from endothelial cells and cells with both fibrogenic and adipogenic potential (CD45^{-}MAC1^{-}TER119^{-}Sca1^{+}). Myogenic tumors resembling human pleomorphic RMS developed only from the satellite cell population (Hettmer et al., 2011; Schulz et al., 2011). Using this strategy, we identified 0.08% of the Tom^{+} muscle interstitial cells from AT mice were within the satellite cell population, in contrast to 18% of Tom^{-} cells. Instead, 92% of Tom^{+} cells were Sca1^{+} (Figure S3G) and 96% of these Tom^{+}Sca1^{+} cells were also PECAM1^{+} (Figure S3H). Since fibroadipogenic progenitors are also contained within the Sca1^{+} population, we evaluated gene expression on cells sorted for both Tomato and Sca1 fluorescence (Figure S3I). Tom^{+}Sca1^{+} cells expressed endothelial markers *Pecam1* and *Tek*, and not the fibroadipogenic marker *Pdgfra*. Consistent with satellite cells being among the

Tom$^-$ population, sorted Tom$^-$Sca1$^-$ cells also expressed *Pax7* and *Myf5* (Figure S3J). Thus, the *aP2-Cre* labeled cells within the skeletal muscle are endothelial cells and previously did not give rise to myogenic sarcomas with oncogenic Kras^{G12V}.

Oncogenic Kras drives angiosarcoma in *aP2-Cre* expressing cells

Next, we investigated whether other drivers of RMS similarly transform *aP2-Cre* expressing cells *in vivo*. Ras mutations and *CDKN2A* loss are common in FN-RMS (Chen et al., 2013b; Paulson et al., 2011; Shern et al., 2014). Thus, we bred *aP2-Cre;LSL-Kras^{G12D};Cdkn2a$^{Flox/Flox}$* compound mutant mice to conditionally activate oncogenic Ras signaling and delete *Cdkn2a* in *aP2-Cre* expressing cells. These mice did not develop RMS but instead all mice developed hemorrhagic tumors in multiple organs including skeletal muscle, lung, heart and adipose with median onset of 29 days (Figures 4A–C). These tumors expressed endothelial markers PECAM1, CD34, PLVAP (Meca32), ERG and KDR, which are diagnostic for angiosarcoma (Figures 4D and S4A). In addition, 2 of the 24 mice developed solid tumors on the lower chest wall one consistent with malignant triton tumor (Figure S4B) and the other pleomorphic spindle cell carcinoma (Figure S4C). These results highlight the dependence of Shh pathway activation by illustrating oncogenic Ras does not phenocopy oncogenic SmoM2 in *aP2-Cre* expressing cells driving FN-RMS, but results in an endothelial tumor. Thus, illustrating that the origin of FN-RMS in the AS mice are distinct from reported Ras-driven models.

SmoM2 promotes a myogenic fate switch during endothelial cell development

After identifying *aP2-Cre* labeled muscle interstitial cells are endothelial cells, we next asked whether SmoM2 expression alters their development. We isolated Tom$^+$ and Tom$^-$ cells by FACS from the SCM of adult AST mice (Figure 5A). Tom$^+$ cells express aP2 as well as *Pecam1* and *Tek* (Figure 5B). In addition, *aP2-Cre* labeled cells co-localize with PECAM1 in cross sections and cultured cells from the SCM of AST mice (Figures S5A&B). In contrast, *aP2-Cre* expressing cells did not colocalize with PAX7 and *Pax7* and interstitial cell markers *Pdgfra, Pdgfrb*, *Pw1* and *Ng2* were enriched in the Tom$^-$ fraction (Figures 5B and S5C–D). Neither fraction expressed the mature adipocyte marker *Pparg* (Figure 5B). These results demonstrate that SmoM2 expression does not block endothelial development within the muscle interstitium.

Next, we assessed the fidelity of the Shh pathway in Tom$^+$ cells isolated from the SCM of P21 AST mice. Despite expression of SmoM2, Tom$^+$ cells did not increase expression of Shh pathway genes suggesting mature endothelial cells are not the origin of FN-RMS in the AS model (Figure 5C). As Shh is a key developmental morphogen, we hypothesized that SmoM2 expression in *aP2-Cre* labeled endothelial progenitor cells induces myogenic transdifferentiation. SmoM2 dependent embryonic proliferations at E17.5 were largely MYOD1 positive while PECAM1 was limited to the vasculature (Figure 5D). These findings suggest that prior to endothelial cell terminal differentiation, *aP2-Cre* expressing endothelial progenitor cells undergo a SmoM2-dependent transformation resulting in FN-RMS.

Purified tumor cells express myogenic specification factors critical for head and neck muscle development

Previously we illustrated similarity in the gene expression profile of FN-RMS from *aP2-Cre;Smo*$^{M2/+}$ and *Myogenin-Cre;Smo*$^{M2/+}$ mice (Hatley et al., 2012). We hypothesized that differences between AS and *Myogenin-Cre;Smo*$^{M2/+}$ tumors should reflect their differing cellular origins. 79 genes were enriched (≥ 2 fold, $p < 0.05$) in AS tumors with respect to *Myogenin-Cre;Smo*$^{M2/+}$ tumors (Table S1) and a subset of these genes were involved in angiogenesis and vascular development (Figure S6A).

Given solid tumors contain heterogeneous cell types, we sought to purify tumor cells for further analysis. We digested AST tumors and separated cells with FACS by Tomato fluorescence and PECAM1 staining to isolate *aP2-Cre*-labeled tumor cells from *aP2-Cre*-labeled tumor vasculature and Tom$^-$ stroma. In contrast to the AST SCM where the majority of Tom$^+$ cells were PECAM1$^+$, tumors contained an additional Tom$^+$PECAM1$^-$ population (Figure 6A). Of the cell populations isolated from tumors, only Tom$^+$PECAM1$^-$ cells displayed sphere initiating capacity (Figure 6B). Although both Tom$^+$PECAM1$^-$ and Tom$^+$PECAM1$^+$ populations expressed SmoM2, only Tom$^+$PECAM1$^-$ cells had increased expression of Shh pathway target genes (Figure 6C). Furthermore, myogenic genes were enriched in Tom$^+$PECAM1$^-$ cells whereas Tom$^+$PECAM1$^+$ cells expressed endothelial genes (Figures 6D&E).

To further define cell populations isolated by FACS from AST tumors, we utilized gene expression arrays. Gene expression separated the cell populations into three distinct groups by PCA of Tom$^-$PECAM1$^-$, Tom$^+$PECAM1$^-$ and Tom$^+$PECAM1$^+$ cells (Figure S6B). We first compared the genes enriched in purified Tom$^+$PECAM1$^-$ cells compared to SCM to genes enriched in unsorted tumors from AS mice compared to SCM (Hatley et al., 2012) and found agreement in 55% of 16,957 ortholog gene pairs (Figure S6C). Further validating that Tom$^+$PECAM1$^-$ cells represent the FN-RMS tumor cell population, genes enriched in the Tom$^+$PECAM1$^-$ cells compared to the Tom$^-$PECAM1$^-$ stroma cells closely resembled that of both FN- and FP-RMS cell lines (Figure S6D). To confirm that the Tom$^+$PECAM1$^+$ population represented the tumor endothelial cells, we compared sorted Tom$^+$PECAM1$^+$ cells to Tom$^+$ endothelial cells isolated from AT SCM (Figure 3) and 97% of genes were similarly expressed (Figure S6E). Genes with increased expression in Tom$^+$PECAM1$^+$ cells compared to Tom$^-$PECAM1$^-$ cells were involved in angiogenesis and vasculature development (Figure S6F). Thus, we were able to separate tumor cells (Tom$^+$PECAM1$^-$) and tumor vascular cells (Tom$^+$PECAM1$^+$) from heterogeneous tumor stroma (Tom$^-$PECAM1$^-$) in tumors from AST mice using differential Tomato and PECAM1 labeling.

To explore mechanisms responsible for FN-RMS formation, we further examined gene expression of Tom$^+$PECAM1$^-$ tumor cells. First, we identified 385 genes enriched in Tom$^+$PECAM1$^-$ tumor cells with respect to Tom$^-$PECAM1$^-$ stroma cells (≥ 2 fold increase, $p < 0.05$) including genes encoding a number of transcription factors that regulate development, including the forkhead box transcription factors FOXD1 and FOXF1, Sox family protein SOX9, T-box transcription factor TBX3 and homeobox protein PROX1. Key components of Notch (HEY1, HEYL), Bmp (BMP4) and Wnt (LEF1, LGR4) signaling pathways were also upregulated as were stem cell markers ALDH1A3 and PROX1 (Figure S6G). Gene ontology

analysis of enriched genes identified muscle related processes and muscle cell differentiation among the most significant GO terms (Figure 6F). Muscle cell differentiation genes including the Mrfs *Myod1, Myf5*, *Myf6* and *Myog* were enriched in Tom^{+}PECAM1^{-} cells (Figure 6D & Table S2).

Among genes significantly enriched in Tom^{+}PECAM1^{-} tumor cells with respect to both Tom^{+}PECAM1^{+} endothelial and Tom^{-}PECAM1^{-} stromal cells were *Tbx1*, *Pitx2, Tcf21* and *Msc* (Figure 6G and S6G) which are transcription factors with critical roles in head and neck muscle specification acting upstream of Mrfs (Buckingham, 2017). *Pax3*, whose expression is required for specification of limb and trunk muscles (Buckingham and Relaix, 2007), was not enriched in Tom^{+}PECAM1^{-} cells (Figure S6H). Since *Tbx1* is a known Shh target gene (Garg et al., 2001), we hypothesize that SmoM2 expression in *aP2-Cre* expressing endothelial progenitors induces TBX1 that in turn activates Mrf expression driving rhabdomyosarcomagenesis. Consistent with this, 34% of *aP2-Cre* labeled cells in E15.5 AST embryos expressed *Tbx1* but only 2% express MYOD1 (Figures 6H&I). At E17.5, the *aP2-Cre* labeled cells in AST are MYOD1 positive (Figure 5D) indicating that *Tbx1* expression precedes *Myod1* expression. As only a fraction of the *aP2-Cre* labeled cells co-localized with *Tbx1*, TBX1 is not likely the lone acting factor downstream of SmoM2 and likely there is redundancy with PITX2, TCF21 and MSC.

aP2-Cre;Smo$^{M2/+}$ FN-RMS tumor cells retain evidence of endothelial origin

Genes involved in tube development were also enriched in Tom^{+}PECAM1^{-} tumor cells with respect to Tom^{-}PECAM1^{-} cells (Figures 6F, S6G and Table S2). To explore whether Tom $^{+}$PECAM1^{-} cells retain evidence of their cellular origins we compared the gene profile of Tom^{+}PECAM1^{-} cells with Tom^{+}PECAM1^{+} tumor vasculature. 32 genes were enriched in both Tom^{+}PECAM1^{-} and Tom^{+}PECAM1^{+} cells compared to Tom^{-}PECAM1^{-} tumor stroma including genes involved in angiogenesis and endothelial cell differentiation (Figures 7A&B and Table S3). In addition, genes encoding endothelial cell transcription factors GATA2 and SOX18 and vascular endothelial cadherin CDH5 were among the 32 overlapping genes (Figure 7C). This was most likely not due to contaminating tumor vasculature as *Pecam1* expression was solely observed in Tom^{+}PECAM1^{+} cells (Figure 7C).

Vascular endothelial growth factor (Vegf) signaling mediated by KDR (VEGFR2) regulates aP2 expression in endothelial cells (Elmasri et al., 2009). Consistent with this, KDR expression at E9.5 precedes and then co-localizes with *aP2-Cre* expression at E10.5 in the branchial arches with 31% of Tom^{+} cells colocalized with KDR (Figures 7D–K). Next, we asked whether the cell expansions observed in AST embryos similarly express KDR. At E15.5, 8% of *aP2-Cre* expressing cells colocalize with KDR (Figure 7L). These findings provide further evidence that FN-RMS originate from endothelial progenitor cells in AST mice.

FN-RMS in *Kdr::Cre;Smo$^{M2/+}$* mice

In the trunk and limbs, endothelial cells and skeletal muscle originate from a common KDR and PAX3 expressing progenitor in the somite (Kardon et al., 2002; Motoike et al., 2003). To determine whether head and neck muscles are similarly derived from KDR^{+} cells, we bred

Kdr::Cre;R26-tdTom mice and assessed tomato expression in head and neck muscle and endothelial cells. At P14, both the quad and SCM exhibited tomato fluorescence grossly (Figure 8A). In contrast to AT mice, both PECAM1^{+} endothelial cells and myofibers in both the SCM and quad of *Kdr::Cre;R26-tdTom* mice display native Tomato fluorescence histologically (Figure 8B). Thus, muscle and endothelial cells within the head and neck arise from common *Kdr::Cre* expressing progenitors. Together these data suggest that KDR acts upstream of aP2 in a multipotent progenitor of endothelium and head and neck muscles. As well, *aP2-Cre* expression is restricted to progenitors committed to an endothelial fate.

To determine whether activation of the Shh pathway in KDR expressing cells would result in RMS, we utilized *Kdr::Cre* to drive SmoM2 expression. No *Kdr::Cre;Smo$^{M2/+}$* mice were born alive and those delivered dead had malformed hindlimbs and large umbilical protrusions. Interestingly, E18.5 *Kdr::Cre;Smo$^{M2/+}$* embryos had MYOD1 and MYOGENIN positive small round blue cell proliferations in the same location as the developing FN-RMS in the AS mice (Figure 8C). The MYOD1 positive tumor cells colocalized with Tomato in *Kdr::Cre;Smo$^{M2/+}$;R26-tdTom* mice (Figure 8D). These results highlight that activating Shh signaling in *Kdr* expressing cells leads to similar myogenic lesions and FN-RMS as in AS mice.

DISCUSSION

The use of lineage specific cis-regulatory regions to express *Cre* recombinase to activate the expression of oncogenes and to delete tumor suppressor genes illustrates that the respective lineage is permissive to transformation. It is not surprising that activation of oncogenic RAS in the context of either *Trp53* or *Cdkn2a* loss using myogenic Cre-drivers results in transformation and myogenic tumors such as FN-RMS (Kashi et al., 2015). However, the serendipitous finding of FN-RMS in *aP2-Cre;Smo$^{M2/+}$* compound mutant mice offers insight into the development of RMS that could not have been predicted *a priori*. The most surprising aspect of our FN-RMS model is that it results from SmoM2 activation in non-muscle *aP2-Cre* expressing cells and it only occurs exclusively in the head and neck. This allowed us the opportunity to understand the origins of RMS that occurs in tissues devoid of skeletal muscle and the development of RMS in the most common location for RMS, the head and neck.

Through genetic fate mapping we find that *aP2-Cre* is not expressed in skeletal muscle but in endothelial cells within the muscle interstitium. Activation of oncogenic SmoM2 with *aP2-Cre* reprogrammed *aP2-Cre* labeled interstitial endothelial progenitor cells leading to FN-RMS formation only in the head and neck. This suggests that expression of SmoM2 in endothelial progenitor cells within the muscle interstitium results in a myogenic fate switch and FN-RMS formation. Consistent with these results, isolated tumor cells are enriched in transcription factors involved in both myogenic specification as well as endothelial cell regulation. Interestingly, recent work using chromatin conformation capture to map topographical associating domains and characterization of the *Foxo1* enhancer speculates a vascular origin in *PAX3-FOXO1* driven fusion–positive RMS (Vicente-Garcia et al., 2017).

Although our characterization focused on skeletal muscle, the expression of *aP2-Cre* in endothelial cells including the adipose vasculature (Jeffery et al., 2014) would account for the occurrence of FN-RMS in adipose in both AS mice (Hatley et al., 2012) as well as *Fabp4-Cre;Smo*$^{M2/+}$ embryos (Nosavanh et al., 2015). Shh pathway responsiveness is reduced in postnatal vasculature, (Passman et al., 2008) and we similarly observed that mature endothelial cells within skeletal muscle do not respond to hedgehog signaling despite the expression of constitutively active Smoothened. These results suggest that SmoM2 promotes myogenic transdifferentitation during a permissive window during endothelial cell development. Supporting this developmental competence model, *Fabp4-Cre;Ptch1*$^{flox/-}$ embryos, in which Shh pathway activation was achieved by conditional deletion of *Ptch1*, similarly develop myogenic lesions within the ventral neck (Nosavanh et al., 2015) whereas *aP2-Cre;LSL-Kras*^{G12D}*;Cdkn2a*$^{Flox/Flox}$ mice develop angiosarcoma and not FN-RMS.

Previously, KDR^{+} cells were shown to contribute to limb skeletal muscle and cardiac muscles development as well as that of endothelial and hematopoietic lineages (Kardon et al., 2002; Motoike et al., 2003). β-galactosidase staining is evident in skeletal muscle from *Kdr::Cre;R26-LacZ* compound mutant mice but not *Kdr::LacZ* knock-in mice indicating that skeletal muscle is derived from a KDR^{+} cell that no longer expresses KDR (Motoike et al., 2003). Our results with *Kdr::Cre;R26-tdTom* mice show that endothelial cells and skeletal muscle within the head and neck are similarly derived from KDR^{+} cells. Lineage tracing and clonal analysis demonstrate that both branchiometric neck skeletal muscle and the second heart field within the pharyngeal mesoderm are derived from a common progenitor (Harel et al., 2009; Lescroart et al., 2015). Within the second heart field in the pharyngeal mesoderm, KDR along with ISL1 and NKX2.5 label a progenitor cell capable of giving rise to cardiac muscle, smooth muscle and endothelial cells (Moretti et al., 2006). Thus, the KDR^{+} multipotent progenitor upstream of *aP2-Cre* in the branchial arches are potentially derived from the second heart field (Diogo et al., 2015; Lescroart et al., 2015). Although KDR signaling regulates aP2 expression in endothelial cells (Elmasri et al., 2009) and *aP2-Cre* is expressed during embryonic development (Urs et al., 2006), our results clearly demonstrate that *aP2-Cre* expressing cells do not contribute to the myogenic lineage and therefore *aP2-Cre* is not expressed in this KDR^{+} early multipotent progenitor population. However, our findings that KDR expression precedes *aP2-Cre* expression in KDR expressing cells within the branchial arch instead suggests *aP2-Cre* is expressed in KDR^{+} committed endothelial progenitors (Figure 8E).

In KDR^{+} bipotent progenitors of the developing trunk and limb, an equilibrium between the transcriptional activity of FOXC1/C2 and PAX3 dictates endothelial or skeletal muscle fate respectively, thus illustrating cellular pliancy of the KDR^{+} progenitors (Lagha et al., 2009). Our results suggest that aberrant Shh pathway activation mediated by SmoM2 leads to transdifferentation of *aP2-Cre* expressing committed endothelial progenitor cells in the head and neck into myoblast-like cells in a manner analogous to increased PAX3 expression in trunk and limb progenitors (Figure 8F).

Distinct transcription factors including TBX1, PITX2, TCF21, and MSC drive specification of head and neck skeletal muscle and regulate Mrf expression (Buckingham, 2017; Kelly et al., 2004; Lu et al., 2002; Shih et al., 2007). Interestingly, *Tbx1*, *Pitx2*, *Tcf21* and *Msc* are

enriched in FN-RMS cells isolated from AST tumors. The Shh pathway activates *Tbx1* expression (Garg et al., 2001) and our findings that TBX1 is expressed prior to MYOD1 in embryonic expansions of *aP2-Cre* expressing cells are consistent with constitutive Hh signaling driving transdifferentiation of *aP2-Cre* expressing endothelial progenitor cells by increasing TBX1 and consequently, Mrf expression (Figure 8F). In addition, TBX1 negatively regulates *Kdr* expression (Lania et al., 2015), and thus may further suppress endothelial cell fate. However, Shh activation occurs after endothelial specification in our AS model of FN-RMS resulting in these cells lacking developmental priming necessary for terminal skeletal muscle differentiation and thus resemble an arrested state of skeletal muscle development.

This work offers a more complete understanding of the intersection between normal development and RMS. As we continue to interrogate the genomics of RMS, it is becoming clear that FN-RMS is likely driven by many distinct genetic events resulting in similar histology. As we strive for more for personalized medicine, including agents to differentiate pediatric embryonal tumors, increased understanding of the developmental underpinnings for these tumors becomes even more critical. For example, FN-RMS in the head and neck derived from endothelial progenitors may not respond to a “differentiation therapy” identified in a Ras-driven tumor of satellite cell origin. Further work investigating likely multiple cellular origins of RMS will compliment extensive genomic analysis to provide therapeutic insights to improve clinical outcomes.

STAR Methods

Contact for Reagent and Resource Sharing

Further information and requests for resources and reagents should be directed to and will be fulfilled by the Lead Contact Mark Hatley (mark.hatley@stjude.org).

Experimental model and subject details

Mouse strains—All mouse strains used have been previously reported: *aP2-Cre* (Tang et al., 2008), *Adipoq-Cre* (#10803, Jackson Laboratories) (Eguchi et al., 2011), *Ucp1-Cre* (#24670, Jackson Laboratories) (Kong et al., 2014), *Fabp4-Cre* (#5069, Jackson Laboratories) (He et al., 2003), *Flk1::Cre (Kdr::Cre)* (#018976, Jackson Laboratories) (Motoike et al., 2003), *R26-mTmG* (#7676, Jackson Laboratories) (Muzumdar et al., 2007), *R26-tdTomato* (#7914, Jackson Laboratories) (Madisen et al., 2010), *R26-LacZ* (#3474, Jackson Laboratories) (Soriano, 1999), *SmoM2* (#5130, Jackson Laboratories) (Mao et al., 2006), *LSL-Kras^{G12D}* (#8179, Jackson Laboratories) (Jackson et al., 2001) and *Cdkn2A^{Flox}* (Aguirre et al., 2003). For Kaplan-Meier tumor free survival analysis, *Adipoq-Cre;Smo$^{M2/+}$* and *Ucp1-Cre;Smo$^{M2/+}$* animals were observed from birth and confirmed to be tumor free at necropsy. For Kaplan-Meier survival analysis, *aP2-Cre; LSL-Kras^{G12D} and aP2-Cre; LSL-Kras^{G12D};Cdkn2a$^{Flox/Flox}$* animals were observed from birth and sacrificed when showing signs of obvious tumor burden or other distress. Full necropsies were performed. All experimental procedures involving animals were reviewed and approved by SJCRH Institutional Animal Care and Use Committee.

Method Details

Histology and immunostaining—Dissected tissues were submerged in PBS and whole mount images acquired on Nikon SMZ 1500 and Leica M165FC fluorescent stereomicroscopes using Nikon Elements and Leica Application Suite X software. Frozen sections were prepared by fixing tissues overnight in 4% paraformaldehyde (PFA) and cryoprotecting in 30% Sucrose, 2 mM $MgCl_2$. Soft tissues were mounted in tissue freezing medium (#TFM-5, General Data) and muscle/tumors snap frozen in 2-methyl-butane cooled in liquid nitrogen prior to sectioning using a conventional cryostat. Formalin fixed Paraffin-embedded (FFPE) sections were prepared by fixation in 10% neutral-buffered formaldehyde (NBF) before embedding in paraffin. Embryos and animals for head and neck sectioning were initially fixed in 4% PFA by transcardial perfusion, and head and neck sections decalcified for 48 hours in CAL-RITE (#5501 Richard Allan Scientific) prior to embedding. Hematoxylin and eosin (H&E) and immunostaining were performed using standard procedures. Dual *Tbx1* RNAscope (#481919, Advanced Cell Diagnostics) and IHC were carried out according to manufacturer's instructions. Antibody concentrations and antigen retrieval conditions are listed in Table S4. Images were captured on Nikon Eclipse 80i upright and Nikon C2 confocal microscopes using Nikon Elements software.

Fluorescent Activated Cell Sorting—Mononuclear cells were isolated from the SCM of 3–4 week old AT or AST animals and tumors from AST animals. For each experiment, SCM was pooled from two aged matched litters. Adjacent adipose was removed from SCM and normal muscle from tumors prior to dissociation. Tissues were manually dissociated and then digested for 1 hour at 37°C in 2 U/mL Collagenase B (#11088831001, Roche)/Dispase II (#04942078001, Roche), 50mM HEPES/KOH pH 7.4; 150 mM NaCl. Following the addition of 2X volume 10% fetal bovine serum (FBS) (#SH30910.03, GE Hyclone) in phosphate buffered saline (PBS) to inactive digestion enzymes, samples were sequentially filtered through 70 μm (#22363548, Fisher) and 40 μm (#22363547, Fisher) filters to yield single cell suspensions. Single cells were blocked in 5% FBS in PBS and then stained for 30 minutes on ice prior to sorting on a FACS Aria Cellsorter (BD Biosciences). Data was acquired and analyzed using FACSDiva software. Antibody concentrations are listed in Table S5 and DAPI used as a live/dead cell marker.

Cell culture and differentiation assays—Primary mouse myoblasts were isolated from hindlimb muscles of 3–4 week old *aP2-Cre;R26-LacZ* mice by manual disassociation and subsequent digestion for 90 minutes in 0.15 U/mL Liberase DL (#0540116000, Roche) at 37°C. Digestion was stopped by the addition of 1X volume 20% FBS in PBS and then samples were sequentially filtered through 100 μm (#352360, BD Falcon) and 70 μm (#22363548, Fisher) filters to yield a single cell suspension. Myoblasts were enriched from cell suspensions after pre-plating for 2 hours. Unadherred cells were cultured in Hams F10 medium (#10070CV, Corning) supplemented with 20% Cosmic Calf serum (#SH30087.03, GE Hyclone), 1% penicillin, streptomycin and amphotericin (PSA) (#A5955, Sigma Aldrich) and 4ng/mL fibroblast growth factor (FGF) (#233-FB-025, R&D systems) on 1% gelatin coated plates at 37°C in 5% CO_2. For differentiation assays, myoblasts were grown until 90% confluence and transferred to DMEM (#SH30243, GE Hyclone) containing 2% horse serum. Following differentiation, cells were fixed for 15 minutes in 4% PFA, 0.1 M

phosphate buffer (pH 7.4), 0.01% sodium deoxycholate, and 0.02% Nonidet P-40 and stained for β-galactosidase activity overnight in 1 mg/mL X-gal (5-bromo-4-chloro-3-indoyl-β-D-galactoside), 5 mM potassium ferricyanide, and 5 mM potassium ferrocyanide, 2 mM $MgCl_2$, 0.01% sodium deoxycholate, and 0.02% Nonidet P-40. Cells transduced with Ad5CMVeGFP (VVC-U of Iowa-4, University of Iowa, Iowa City, IA, USA) prior to differentiation were utilized as a positive control for β-galactosidase staining. Mononuclear cells were isolated from SCM of 3–4 week old AT and AST animals by digesting disassociated tissue in 2 U/mL Collagenase B (#11088831001, Roche)/Dispase II (#04942078001, Roche) and then culturing until confluent in DMEM (#SH30243, GE Hyclone) supplemented with 10% FBS (#SH30910.03 GE Hyclone) and 1% PSA (#A5955, Sigma Aldrich). Immunofluorescence was performed according to standard techniques using antibodies listed in Table S4. Tumor spheres were grown on ultra low attachment plates (#3471, Corning) in neurobasal medium (#12348 Gibco) supplemented 10 ng/mL epidermal growth factor (#23626, R and D systems), 20 ng/mL FGF (#233-FB-025, R and D systems), 2x B27 supplement (#17504-44, Gibco), 1x Glutamax (#35050, Gibco) and 1% PSA (#A5955, Sigma Aldrich) with from cell populations isolated from AST tumors by FACS. Images were captured on a Nikon Eclipse Ti-S inverted microscope using Nikon Elements Software.

RNA isolation and Gene Expression analysis—Total RNA was isolated from whole tissues using a miRNEasy mini kit (#217004, Qiagen, Valencia, CA, USA) and from sorted cell populations using a miRNEasy micro kit (#217084, Qiagen) according to manufacturer's instructions. Reverse transcription was performed using Superscript III First Strand Synthesis using random hexamer primers. Real-time PCR was performed utilizing SYBR primers and Taqman probes listed in Table S6 or Key Resources Table and normalized to *Actb* expression. Relative quantity of *tomato* expression was determined using the ΔCT method and of other genes of interest using the ΔΔCT method.

For gene expression profiling, amplified cDNA was prepared using the Ovation Pico WTA System V2 (#3302, Nugen, San Carlos, CA, USA) from RNA isolated from sorted cell populations. Gene expression analysis was performed on Mouse gene 2.0 ST microarrays (#902118, Affymetrix, Santa Clara, CA, USA). Data were imported into Partek Genome Suite 6.6, visualized by principal component analysis to check for consistency of samples and class variance. Data were then batch corrected and statistically tested using an unequal variance t test. After filtering unannotated transcripts, transcripts were imported into STATA/MP 14.2 and p-values adjusted for multiple comparisons by the Benjamini-Hochberg FDR method (Benjamini and Hochberg, 1995). Volcano plots were produced in STATA/MP 14.2 by plotting the Log_{10} transformed p value from the unequal variance t test against the Log ratio of expression for datasets being compared. Array data is deposited in GEO database (GSE98059). The gene expression profile of Tom^+ and Tom^- cells isolated from AT SCM were compared to microvascular endothelial cells (GSE47067) (Nolan et al., 2013), satellite cells and $PW1^+$ interstitial cells (GSE40523) (Pannerec et al., 2013) as well as brown and white adipose (GSE8044) (Seale et al., 2007). The gene expression profile of $Tom^+PECAM1^-$ cells isolated from AST tumors were expressed relative to normal SCM from C57BL/6 animals (GSE85834) (Hanna et al., 2017) and compared to that of whole

aP2-Cre;Smo$^{M2/+}$ tumors normalized to SCM (GSE40359) (Hatley et al., 2012). Comparisons between the gene expression profile of Tom^{+}PECAM1^{+} cells isolated from AST tumors and Tom^{+} cells isolated from AT SCM (this study) were also made. Gene Ontology analysis was performed using Enrichr gene enrichment analysis tool (Chen et al., 2013a; Kuleshov et al., 2016). Reported p values are adjusted using the Benjamini-Hochberg method.

Quantification and Statistical Analysis

Sample size and replicates for each experiment are listed in the figure legends. Embryonic expansions of *aP2-Cre* expressing cells (Figure 2) were defined as tomato positive cell proliferations that displaced and engulfed the MHC+ myofibres. Real-time PCR error bars indicate SEM of three independent biological experiments performed in technical replicate using two tailed unpaired student t tests for pairwise comparisons (Graphpad Prism6). Kaplan-Meier survival analysis was performed by Log Rank (Mantel-Cox) test. p values less than 0.05 were considered significant.

Data Availability

The microarray data has been deposited in the Gene Expression Omnibus database under number GSE98059.

Supplementary Material

Refer to Web version on PubMed Central for supplementary material.

Acknowledgments

We thank Shannon McKinney-Freeman for mouse generosity. We also wish to thank St. Jude Children's Research Hospital Cancer Center shared resources including Cell and Tissue Imaging (Victoria Frohlich, Jennifer Peters), Flow Cytometry and Cell Sorting (Richard Ashmun), Veterinary Pathology (Peter Vogel, Dorothy Bush, Sean Savage) and the Hartwell Center and Functional Genomics (Melanie Lloyd) as well as Jonathan Go for technical assistance. Work in M.E.H.'s laboratory is supported by the V Foundation for Cancer Research, NIH (NCI-R01CA216344 and K08CA151649), St. Jude Cancer Center Support Grant (P30 CA021765), and American Lebanese Syrian Associated Charities of St. Jude Children's Research Hospital.

References

Aguirre AJ, Bardeesy N, Sinha M, Lopez L, Tuveson DA, Horner J, Redston MS, DePinho RA. Activated Kras and Ink4a/Arf deficiency cooperate to produce metastatic pancreatic ductal adenocarcinoma. Genes Dev. 2003; 17:3112–3126. [PubMed: 14681207]

Benjamini Y, Hochberg Y. Controlling the False Discovery Rate: A Practical and Powerful Approach to Multiple Testing. Journal of the Royal Statistical Society Series B (Methodological). 1995; 57:289–300.

Blum JM, Ano L, Li Z, Van Mater D, Bennett BD, Sachdeva M, Lagutina I, Zhang M, Mito JK, Dodd LG, et al. Distinct and overlapping sarcoma subtypes initiated from muscle stem and progenitor cells. Cell reports. 2013; 5:933–940. [PubMed: 24239359]

Borycki AG, Brunk B, Tajbakhsh S, Buckingham M, Chiang C, Emerson CP Jr. Sonic hedgehog controls epaxial muscle determination through Myf5 activation. Development. 1999; 126:4053–4063. [PubMed: 10457014]

Bridge JA, Liu J, Weibolt V, Baker KS, Perry D, Kruger R, Qualman S, Barr F, Sorensen P, Triche T, Suijkerbuijk R. Novel genomic imbalances in embryonal rhabdomyosarcoma revealed by

comparative genomic hybridization and fluorescence in situ hybridization: an intergroup rhabdomyosarcoma study. Genes, chromosomes & cancer. 2000; 27:337–344. [PubMed: 10719362]

Buckingham M. Gene regulatory networks and cell lineages that underlie the formation of skeletal muscle. Proc Natl Acad Sci U S A. 2017

Buckingham M, Relaix F. The role of Pax genes in the development of tissues and organs: Pax3 and Pax7 regulate muscle progenitor cell functions. Annual review of cell and developmental biology. 2007; 23:645–673.

Buckingham M, Rigby PW. Gene regulatory networks and transcriptional mechanisms that control myogenesis. Dev Cell. 2014; 28:225–238. [PubMed: 24525185]

Chen EY, Dobrinski KP, Brown KH, Clagg R, Edelman E, Ignatius MS, Chen JY, Brockmann J, Nielsen GP, Ramaswamy S, et al. Cross-species array comparative genomic hybridization identifies novel oncogenic events in zebrafish and human embryonal rhabdomyosarcoma. PLoS Genet. 2013a; 9:e1003727. [PubMed: 24009521]

Chen X, Stewart E, Shelat AA, Qu C, Bahrami A, Hatley M, Wu G, Bradley C, McEvoy J, Pappo A, et al. Targeting oxidative stress in embryonal rhabdomyosarcoma. Cancer cell. 2013b; 24:710–724. [PubMed: 24332040]

Davis RJ, D'Cruz CM, Lovell MA, Biegel JA, Barr FG. Fusion of PAX7 to FKHR by the variant t(1;13)(p36;q14) translocation in alveolar rhabdomyosarcoma. Cancer Res. 1994; 54:2869–2872. [PubMed: 8187070]

Diogo R, Kelly RG, Christiaen L, Levine M, Ziermann JM, Molnar JL, Noden DM, Tzahor E. A new heart for a new head in vertebrate cardiopharyngeal evolution. Nature. 2015; 520:466–473. [PubMed: 25903628]

Eguchi J, Wang X, Yu S, Kershaw EE, Chiu PC, Dushay J, Estall JL, Klein U, Maratos-Flier E, Rosen ED. Transcriptional control of adipose lipid handling by IRF4. Cell Metab. 2011; 13:249–259. [PubMed: 21356515]

Elmasri H, Karaaslan C, Teper Y, Ghelfi E, Weng M, Ince TA, Kozakewich H, Bischoff J, Cataltepe S. Fatty acid binding protein 4 is a target of VEGF and a regulator of cell proliferation in endothelial cells. FASEB J. 2009; 23:3865–3873. [PubMed: 19625659]

Galili N, Davis RJ, Fredericks WJ, Mukhopadhyay S, Rauscher FJ 3rd, Emanuel BS, Rovera G, Barr FG. Fusion of a fork head domain gene to PAX3 in the solid tumour alveolar rhabdomyosarcoma. Nature genetics. 1993; 5:230–235. [PubMed: 8275086]

Garg V, Yamagishi C, Hu T, Kathiriya IS, Yamagishi H, Srivastava D. Tbx1, a DiGeorge syndrome candidate gene, is regulated by sonic hedgehog during pharyngeal arch development. Dev Biol. 2001; 235:62–73. [PubMed: 11412027]

Hahn H, Wojnowski L, Zimmer AM, Hall J, Miller G, Zimmer A. Rhabdomyosarcomas and radiation hypersensitivity in a mouse model of Gorlin syndrome. Nat Med. 1998; 4:619–622. [PubMed: 9585239]

Hanna JA, Drummond CJ, Garcia MR, Go JC, Finkelstein D, Rehg JE, Hatley ME. Biallelic Dicer1 loss mediated by aP2-Cre drives angiosarcoma. Cancer Res. 2017

Harel I, Nathan E, Tirosh-Finkel L, Zigdon H, Guimaraes-Camboa N, Evans SM, Tzahor E. Distinct origins and genetic programs of head muscle satellite cells. Dev Cell. 2009; 16:822–832. [PubMed: 19531353]

Hatley ME, Tang W, Garcia MR, Finkelstein D, Millay DP, Liu N, Graff J, Galindo RL, Olson EN. A mouse model of rhabdomyosarcoma originating from the adipocyte lineage. Cancer cell. 2012; 22:536–546. [PubMed: 23079662]

He W, Barak Y, Hevener A, Olson P, Liao D, Le J, Nelson M, Ong E, Olefsky JM, Evans RM. Adipose-specific peroxisome proliferator-activated receptor gamma knockout causes insulin resistance in fat and liver but not in muscle. Proc Natl Acad Sci U S A. 2003; 100:15712–15717. [PubMed: 14660788]

Hettmer S, Liu J, Miller CM, Lindsay MC, Sparks CA, Guertin DA, Bronson RT, Langenau DM, Wagers AJ. Sarcomas induced in discrete subsets of prospectively isolated skeletal muscle cells. Proc Natl Acad Sci U S A. 2011; 108:20002–20007. [PubMed: 22135462]

Jackson EL, Willis N, Mercer K, Bronson RT, Crowley D, Montoya R, Jacks T, Tuveson DA. Analysis of lung tumor initiation and progression using conditional expression of oncogenic K-ras. Genes Dev. 2001; 15:3243–3248. [PubMed: 11751630]

Jeffery E, Berry R, Church CD, Yu S, Shook BA, Horsley V, Rosen ED, Rodeheffer MS. Characterization of Cre recombinase models for the study of adipose tissue. Adipocyte. 2014; 3:206–211. [PubMed: 25068087]

Kardon G, Campbell JK, Tabin CJ. Local extrinsic signals determine muscle and endothelial cell fate and patterning in the vertebrate limb. Dev Cell. 2002; 3:533–545. [PubMed: 12408805]

Kashi VP, Hatley ME, Galindo RL. Probing for a deeper understanding of rhabdomyosarcoma: insights from complementary model systems. Nat Rev Cancer. 2015; 15:426–439. [PubMed: 26105539]

Kelly RG, Jerome-Majewska LA, Papaioannou VE. The del22q11.2 candidate gene Tbx1 regulates branchiomeric myogenesis. Hum Mol Genet. 2004; 13:2829–2840. [PubMed: 15385444]

Kong X, Banks A, Liu T, Kazak L, Rao RR, Cohen P, Wang X, Yu S, Lo JC, Tseng YH, et al. IRF4 is a key thermogenic transcriptional partner of PGC-1alpha. Cell. 2014; 158:69–83. [PubMed: 24995979]

Kuleshov MV, Jones MR, Rouillard AD, Fernandez NF, Duan Q, Wang Z, Koplev S, Jenkins SL, Jagodnik KM, Lachmann A, et al. Enrichr: a comprehensive gene set enrichment analysis web server 2016 update. Nucleic Acids Res. 2016; 44:W90–97. [PubMed: 27141961]

Lagha M, Brunelli S, Messina G, Cumano A, Kume T, Relaix F, Buckingham ME. Pax3:Foxc2 reciprocal repression in the somite modulates muscular versus vascular cell fate choice in multipotent progenitors. Dev Cell. 2009; 17:892–899. [PubMed: 20059958]

Lania G, Ferrentino R, Baldini A. TBX1 Represses Vegfr2 Gene Expression and Enhances the Cardiac Fate of VEGFR2+ Cells. PLoS One. 2015; 10:e0138525. [PubMed: 26382615]

Lee KY, Russell SJ, Ussar S, Boucher J, Vernochet C, Mori MA, Smyth G, Rourk M, Cederquist C, Rosen ED, et al. Lessons on conditional gene targeting in mouse adipose tissue. Diabetes. 2013; 62:864–874. [PubMed: 23321074]

Lee Y, Kawagoe R, Sasai K, Li Y, Russell HR, Curran T, McKinnon PJ. Loss of suppressor-of-fused function promotes tumorigenesis. Oncogene. 2007; 26:6442–6447. [PubMed: 17452975]

Lescroart F, Hamou W, Francou A, Theveniau-Ruissy M, Kelly RG, Buckingham M. Clonal analysis reveals a common origin between nonsomite-derived neck muscles and heart myocardium. Proc Natl Acad Sci U S A. 2015; 112:1446–1451. [PubMed: 25605943]

Lindahl P, Johansson BR, Leveen P, Betsholtz C. Pericyte loss and microaneurysm formation in PDGF-B-deficient mice. Science. 1997; 277:242–245. [PubMed: 9211853]

Liu N, Garry GA, Li S, Bezprozvannaya S, Sanchez-Ortiz E, Chen B, Shelton JM, Jaichander P, Bassel-Duby R, Olson EN. A Twist2-dependent progenitor cell contributes to adult skeletal muscle. Nat Cell Biol. 2017; 19:202–213. [PubMed: 28218909]

Lu JR, Bassel-Duby R, Hawkins A, Chang P, Valdez R, Wu H, Gan L, Shelton JM, Richardson JA, Olson EN. Control of facial muscle development by MyoR and capsulin. Science. 2002; 298:2378–2381. [PubMed: 12493912]

Madisen L, Zwingman TA, Sunkin SM, Oh SW, Zariwala HA, Gu H, Ng LL, Palmiter RD, Hawrylycz MJ, Jones AR, et al. A robust and high-throughput Cre reporting and characterization system for the whole mouse brain. Nat Neurosci. 2010; 13:133–140. [PubMed: 20023653]

Malecova B, Puri PL. “Mix of Mics”-Phenotypic and Biological Heterogeneity of “Multipotent” Muscle Interstitial Cells (MICs). J Stem Cell Res Ther. 2012

Mao J, Ligon KL, Rakhlin EY, Thayer SP, Bronson RT, Rowitch D, McMahon AP. A novel somatic mouse model to survey tumorigenic potential applied to the Hedgehog pathway. Cancer Res. 2006; 66:10171–10178. [PubMed: 17047082]

Mathew SJ, Hansen JM, Merrell AJ, Murphy MM, Lawson JA, Hutcheson DA, Hansen MS, Angus-Hill M, Kardon G. Connective tissue fibroblasts and Tcf4 regulate myogenesis. Development. 2011; 138:371–384. [PubMed: 21177349]

Michailovici I, Eigler T, Tzahor E. Craniofacial Muscle Development. Curr Top Dev Biol. 2015; 115:3–30. [PubMed: 26589919]

Moretti A, Caron L, Nakano A, Lam JT, Bernshausen A, Chen Y, Qyang Y, Bu L, Sasaki M, Martin-Puig S, et al. Multipotent embryonic isl1+ progenitor cells lead to cardiac, smooth muscle, and endothelial cell diversification. Cell. 2006; 127:1151–1165. [PubMed: 17123592]

Motoike T, Markham DW, Rossant J, Sato TN. Evidence for novel fate of Flk1+ progenitor: contribution to muscle lineage. Genesis. 2003; 35:153–159. [PubMed: 12640619]

Munsterberg AE, Kitajewski J, Bumcrot DA, McMahon AP, Lassar AB. Combinatorial signaling by Sonic hedgehog and Wnt family members induces myogenic bHLH gene expression in the somite. Genes Dev. 1995; 9:2911–2922. [PubMed: 7498788]

Muzumdar MD, Tasic B, Miyamichi K, Li L, Luo L. A global double-fluorescent Cre reporter mouse. Genesis. 2007; 45:593–605. [PubMed: 17868096]

Nolan DJ, Ginsberg M, Israely E, Palikuqi B, Poulos MG, James D, Ding BS, Schachterle W, Liu Y, Rosenwaks Z, et al. Molecular signatures of tissue-specific microvascular endothelial cell heterogeneity in organ maintenance and regeneration. Dev Cell. 2013; 26:204–219. [PubMed: 23871589]

Nosavanh L, Yu DH, Jaehnig EJ, Tong Q, Shen L, Chen MH. Cell-autonomous activation of Hedgehog signaling inhibits brown adipose tissue development. Proc Natl Acad Sci U S A. 2015; 112:5069–5074. [PubMed: 25848030]

Oberlin O, Rey A, Lyden E, Bisogno G, Stevens MC, Meyer WH, Carli M, Anderson JR. Prognostic factors in metastatic rhabdomyosarcomas: results of a pooled analysis from United States and European cooperative groups. J Clin Oncol. 2008; 26:2384–2389. [PubMed: 18467730]

Ozerdem U, Grako KA, Dahlin-Huppe K, Monosov E, Stallcup WB. NG2 proteoglycan is expressed exclusively by mural cells during vascular morphogenesis. Dev Dyn. 2001; 222:218–227. [PubMed: 11668599]

Pak E, Segal RA. Hedgehog Signal Transduction: Key Players, Oncogenic Drivers, and Cancer Therapy. Dev Cell. 2016; 38:333–344. [PubMed: 27554855]

Pannerec A, Formicola L, Besson V, Marazzi G, Sassoon DA. Defining skeletal muscle resident progenitors and their cell fate potentials. Development. 2013; 140:2879–2891. [PubMed: 23739133]

Parham DM, Barr FG. Classification of rhabdomyosarcoma and its molecular basis. Advances in anatomic pathology. 2013; 20:387–397. [PubMed: 24113309]

Passman JN, Dong XR, Wu SP, Maguire CT, Hogan KA, Bautch VL, Majesky MW. A sonic hedgehog signaling domain in the arterial adventitia supports resident Sca1+ smooth muscle progenitor cells. Proc Natl Acad Sci U S A. 2008; 105:9349–9354. [PubMed: 18591670]

Paulson V, Chandler G, Rakheja D, Galindo RL, Wilson K, Amatruda JF, Cameron S. High-resolution array CGH identifies common mechanisms that drive embryonal rhabdomyosarcoma pathogenesis. Genes, chromosomes & cancer. 2011; 50:397–408. [PubMed: 21412928]

Perez EA, Kassira N, Cheung MC, Koniaris LG, Neville HL, Sola JE. Rhabdomyosarcoma in children: a SEER population based study. The Journal of surgical research. 2011; 170:e243–251. [PubMed: 21529833]

Pressey JG, Anderson JR, Crossman DK, Lynch JC, Barr FG. Hedgehog pathway activity in pediatric embryonal rhabdomyosarcoma and undifferentiated sarcoma: a report from the Children's Oncology Group. Pediatr Blood Cancer. 2011; 57:930–938. [PubMed: 21618411]

Rubin BP, Nishijo K, Chen HI, Yi X, Schuetze DP, Pal R, Prajapati SI, Abraham J, Arenkiel BR, Chen QR, et al. Evidence for an unanticipated relationship between undifferentiated pleomorphic sarcoma and embryonal rhabdomyosarcoma. Cancer cell. 2011; 19:177–191. [PubMed: 21316601]

Satheesha S, Manzella G, Bovay A, Casanova EA, Bode PK, Belle R, Feuchtgruber S, Jaaks P, Dogan N, Koscielniak E, Schafer BW. Targeting hedgehog signaling reduces self-renewal in embryonal rhabdomyosarcoma. Oncogene. 2016; 35:2020–2030. [PubMed: 26189795]

Schulz TJ, Huang TL, Tran TT, Zhang H, Townsend KL, Shadrach JL, Cerletti M, McDougall LE, Giorgadze N, Tchkonia T, et al. Identification of inducible brown adipocyte progenitors residing in skeletal muscle and white fat. Proc Natl Acad Sci U S A. 2011; 108:143–148. [PubMed: 21173238]

Seale P, Bjork B, Yang W, Kajimura S, Chin S, Kuang S, Scime A, Devarakonda S, Conroe HM, Erdjument-Bromage H, et al. PRDM16 controls a brown fat/skeletal muscle switch. Nature. 2008; 454:961–967. [PubMed: 18719582]

Seale P, Kajimura S, Yang W, Chin S, Rohas LM, Uldry M, Tavernier G, Langin D, Spiegelman BM. Transcriptional control of brown fat determination by PRDM16. Cell metabolism. 2007; 6:38–54. [PubMed: 17618855]

Shern JF, Chen L, Chmielecki J, Wei JS, Patidar R, Rosenberg M, Ambrogio L, Auclair D, Wang J, Song YK, et al. Comprehensive genomic analysis of rhabdomyosarcoma reveals a landscape of alterations affecting a common genetic axis in fusion-positive and fusion-negative tumors. Cancer discovery. 2014; 4:216–231. [PubMed: 24436047]

Shih HP, Gross MK, Kioussi C. Cranial muscle defects of Pitx2 mutants result from specification defects in the first branchial arch. Proc Natl Acad Sci U S A. 2007; 104:5907–5912. [PubMed: 17384148]

Soriano P. Generalized lacZ expression with the ROSA26 Cre reporter strain. Nature genetics. 1999; 21:70–71. [PubMed: 9916792]

Sultan I, Qaddoumi I, Yaser S, Rodriguez-Galindo C, Ferrari A. Comparing adult and pediatric rhabdomyosarcoma in the surveillance, epidemiology and end results program, 1973 to 2005: an analysis of 2,600 patients. J Clin Oncol. 2009; 27:3391–3397. [PubMed: 19398574]

Tagliafico E, Brunelli S, Bergamaschi A, De Angelis L, Scardigli R, Galli D, Battini R, Bianco P, Ferrari S, Cossu G, Ferrari S. TGFbeta/BMP activate the smooth muscle/bone differentiation programs in mesoangioblasts. J Cell Sci. 2004; 117:4377–4388. [PubMed: 15331661]

Tang W, Zeve D, Suh JM, Bosnakovski D, Kyba M, Hammer RE, Tallquist MD, Graff JM. White fat progenitor cells reside in the adipose vasculature. Science. 2008; 322:583–586. [PubMed: 18801968]

Uezumi A, Fukada S, Yamamoto N, Takeda S, Tsuchida K. Mesenchymal progenitors distinct from satellite cells contribute to ectopic fat cell formation in skeletal muscle. Nat Cell Biol. 2010; 12:143–152. [PubMed: 20081842]

Urs S, Harrington A, Liaw L, Small D. Selective expression of an aP2/Fatty Acid Binding Protein 4-Cre transgene in non-adipogenic tissues during embryonic development. Transgenic research. 2006; 15:647–653. [PubMed: 16952017]

Van Mater D, Ano L, Blum JM, Webster MT, Huang W, Williams N, Ma Y, Cardona DM, Fan CM, Kirsch DG. Acute tissue injury activates satellite cells and promotes sarcoma formation via the HGF/c-MET signaling pathway. Cancer Res. 2015; 75:605–614. [PubMed: 25503558]

Vicente-Garcia C, Villarejo-Balcells B, Irastorza-Azcarate I, Naranjo S, Acemel RD, Tena JJ, Rigby PWJ, Devos DP, Gomez-Skarmeta JL, Carvajal JJ. Regulatory landscape fusion in rhabdomyosarcoma through interactions between the PAX3 promoter and FOXO1 regulatory elements. Genome Biol. 2017; 18:106. [PubMed: 28615069]

Williamson D, Missiaglia E, de Reynies A, Pierron G, Thuille B, Palenzuela G, Thway K, Orbach D, Lae M, Freneaux P, et al. Fusion gene-negative alveolar rhabdomyosarcoma is clinically and molecularly indistinguishable from embryonal rhabdomyosarcoma. J Clin Oncol. 2010; 28:2151–2158. [PubMed: 20351326]

Zhang M, Qiu Q, Li Z, Sachdeva M, Min H, Cardona DM, DeLaney TF, Han T, Ma Y, Luo L, et al. HIF-1 Alpha Regulates the Response of Primary Sarcomas to Radiation Therapy through a Cell Autonomous Mechanism. Radiation research. 2015; 183:594–609. [PubMed: 25973951]

Zibat A, Missiaglia E, Rosenberger A, Pritchard-Jones K, Shipley J, Hahn H, Fulda S. Activation of the hedgehog pathway confers a poor prognosis in embryonal and fusion gene-negative alveolar rhabdomyosarcoma. Oncogene. 2010; 29:6323–6330. [PubMed: 20818440]

SIGNIFICANCE

RMS is the most common pediatric soft tissue sarcoma and occurs anywhere in the body including tissues devoid of skeletal muscle. The cell of origin for RMS remains unknown. Identification of the cell lineages that contribute to RMS formation provides insight into the mechanisms of tumorigenesis. We demonstrate using *aP2-Cre* to activate the hedgehog pathway that fusion negative RMS originates from endothelial progenitor cells specifically in the head and neck, the most common location of RMS. Our findings illustrate how normal muscle developmental programs are perturbed to drive location specific tumor formation through transdifferentiation induced by hedgehog activation in endothelial progenitors. These studies implicate cell of origin as a major determinate of RMS location and therefore survival.

HIGHLIGHTS

- Committed endothelial progenitors can give rise to rhabdomyosarcoma (RMS)
- Aberrant activation of muscle development programs in non-myogenic cells drive RMS
- SmoM2 transdifferentiates endothelial progenitors resulting in RMS
- Cell of origin emerges as major determinant of RMS location

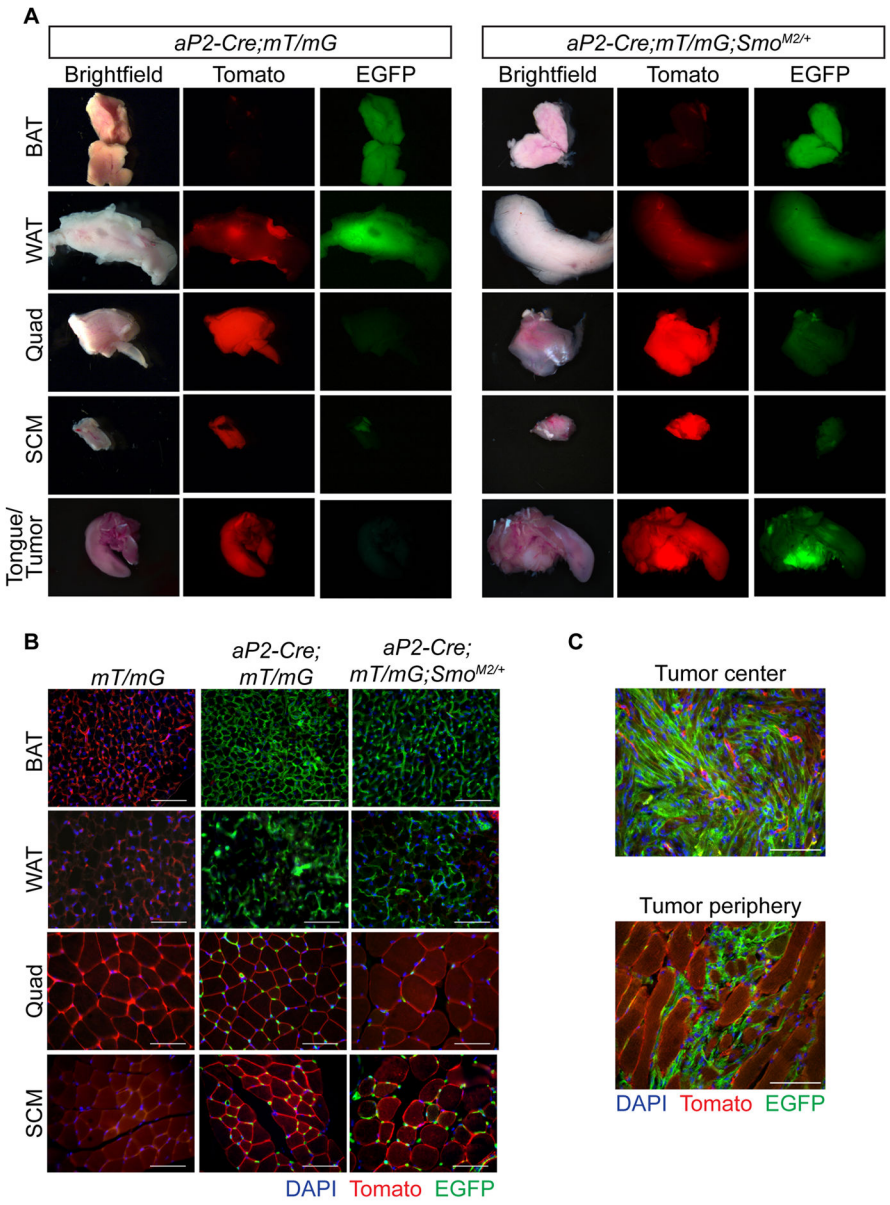

Figure 1. *aP2-Cre* labels cells within both adipose tissue and skeletal muscle

(A) Representative whole mount images of BAT, WAT, quad, SCM and tongue from *aP2-Cre;mT/mG* and *aP2-Cre;mT/mG;Smo*$^{M2/+}$ mice (n = 3). Scale bars, 3 mm. Arrowhead denotes tumor.

(B) Representative tissue sections from *mT/mG*, *aP2-Cre;mT/mG* and *aP2-Cre;mT/mG;Smo*$^{M2/+}$ mice (n = 3). Scale bars, 50 μm.

(C) Representative images of tumor center and tumor periphery of *aP2-Cre;mT/mG;Smo*$^{M2/+}$ mice (n = 3). Scale bars, 50 μm.

See also Figure S1.

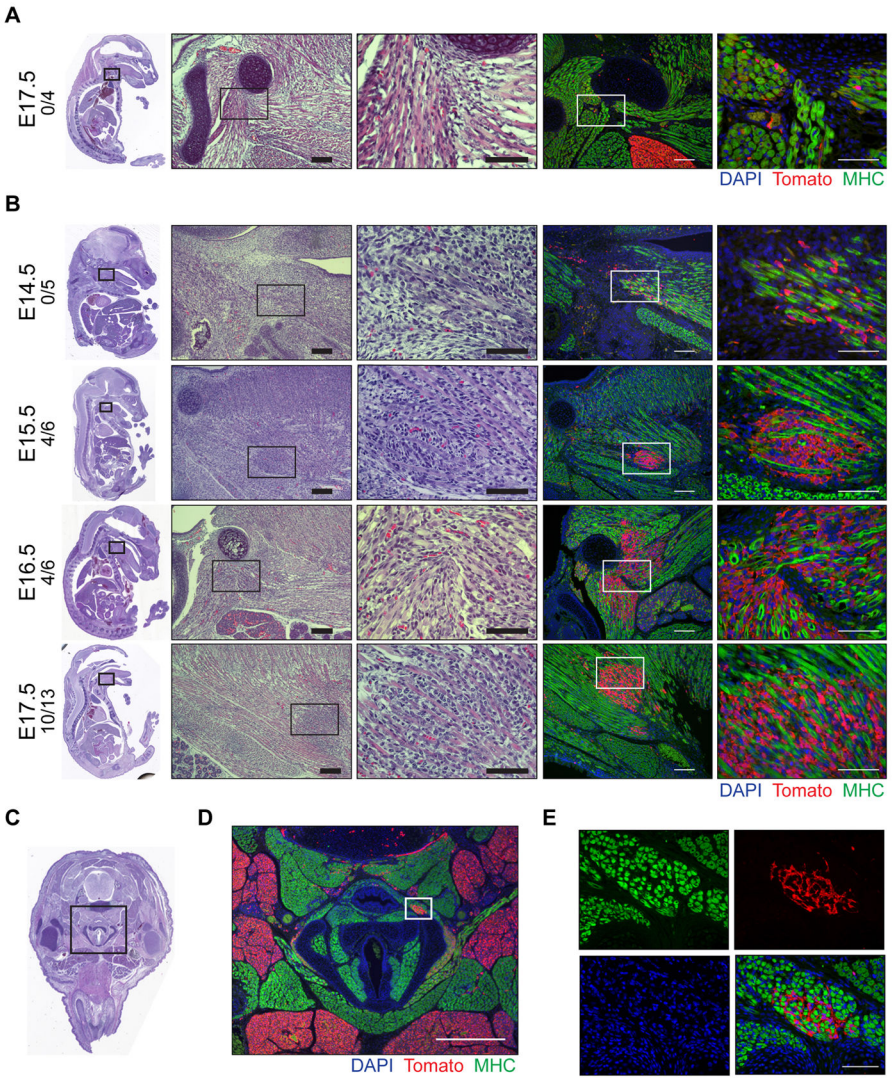

Figure 2. SmoM2 dependent proliferation of *aP2-Cre* labeled cells during embryogenesis

(A–B) Representative H&E and immunostaining of sagittal sections from AT (A) and AST (B) embryos. Embryonic age and number of embryos with Tomato positive expansions/total embryos shown on left. Right panels show high magnification of boxed insets. Scale bars, 100 μm (left) and 50 μm (right).

(C) H&E staining of transverse section of E17.5 AST embryo.

(D) Magnification of boxed inset from (C) of AST embryo immunostained as in (A). Scale bar, 500 μm.

(E) Magnification of boxed inset (D) of AST embryo immunostained as in (A)(n = 3). Scale bar, 50 μm.

* denotes regions of adipose.

See also Figure S2.

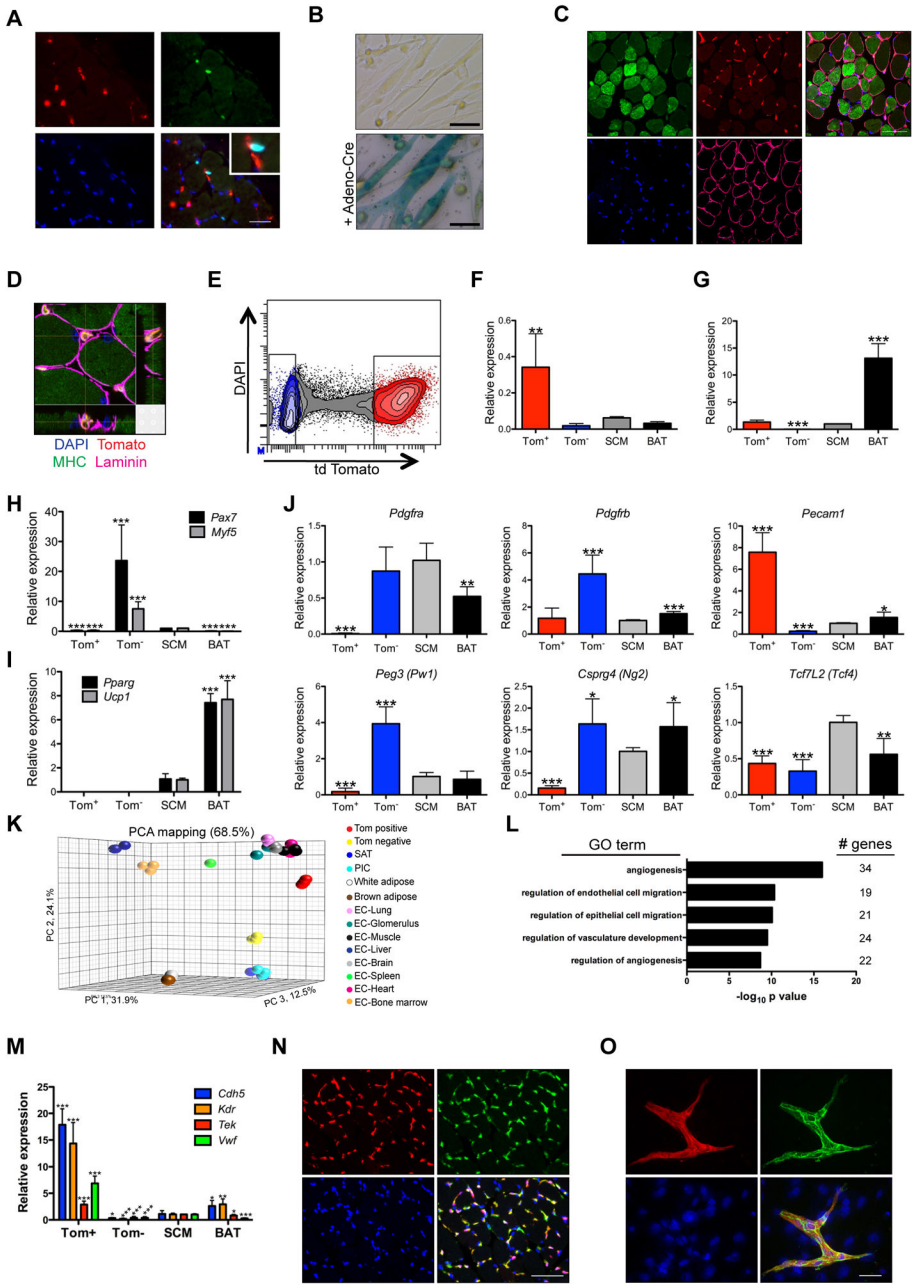

Figure 3. *aP2-Cre* labels endothelial cells within skeletal muscle interstitium

(A) Immunostaining of AT SCM cross sections illustrating Tomato (red, arrowheads), PAX7 (green, arrows), DAPI (blue) positive cells (high magnification inset shown)(n = 3). Scale bars, 25 μm.

(B) β-galactosidase staining of myoblasts isolated from *aP2-Cre;R26-LacZ* mice following *in vitro* differentiation. Cells infected with adeno-Cre as control (n = 3). Scale bars, 50 μm.

(C) Immunostaining of AT SCM cross sections showing Tomato (red), MHC (green), LAMININ (magenta) and DAPI (blue)(n = 3). Scale bar, 50 μm.

(D) Confocal microscopy of (C) illustrating 3D cross sections with Tomato labeled cells in muscle interstitium. Scale bar, 10 μm.

(E–F) Isolation of Tom^+ and Tom^- cells from AT SCM by FACS (E) and confirmation by real-time PCR for Tomato (F). Data shown are normalized to *Actb* (n = 3, mean ± SEM).

(G–J) Gene expression by real-time PCR from Tom^+ and Tom^- cells isolated as in (E) in comparison to mature SCM and BAT from $Smo^{M2/M2}$ mice: aP2 (G), myogenic genes *Myf5* and *Pax7* (H), adipose genes *Pparg* and *Ucp1* (I), and muscle interstitial cell genes (J). Data shown are normalized to *Actb* expression and expressed relative to SCM (n = 3, mean ± SEM).

(K) Principle component analysis of Tom^+ and Tom^- cells isolated as in (E), microvascular endothelial cells, satellite cells, $PW1^+$ interstitial cells (PICs) and adipose. Coordinates describe 68.5% of the data.

(L) Gene ontology analysis of genes enriched in Tom^+ vs Tom^- cells isolated as in (E).

(M) Expression of endothelial genes in Tom^+ and Tom^- cells isolated as in (E) by real-time PCR. Data analyzed as in (G)(n = 3, mean ± SEM).

(N) Immunostaining of AT SCM cross sections showing Tomato (red), PECAM1 (green), DAPI (blue) (n = 2). Scale bar, 50 μm.

(O) Immunocytochemistry of cells isolated from AT SCM and grown to confluence showing Tomato (red), PECAM1 (green), DAPI (blue) (n = 4). Scale bar, 50 μm.

*$p < 0.05$, ** $p < 0.01$, *** $p < 0.001$.

See also Figure S3.

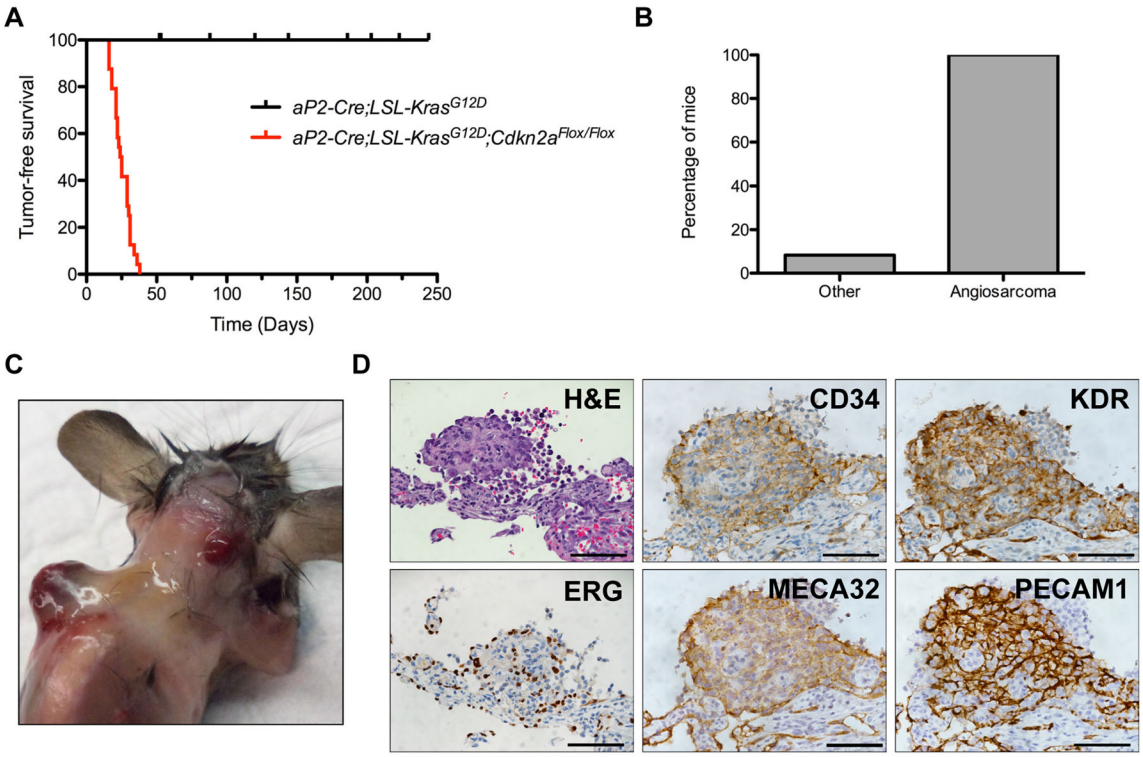

Figure 4. Oncogenic KRAS drives angiosarcoma in *aP2-Cre* expressing cells

(A) Kaplan-Meier survival curve illustrating survival of *aP2-Cre;LSL-Kras^{G12D};Cdkn2a$^{Flox/Flox}$*(n = 24) and *aP2-Cre;LSL-Kras^{G12D}*(n = 10) mice. $p < 0.0001$.

(B) Percentage of *aP2-Cre;LSL-Kras^{G12D};Cdkn2a$^{Flox/Flox}$* mice developing angiosarcoma or other malignancies.

(C) Angiosarcomas (arrowheads) in *aP2-Cre;LSL-Kras^{G12D};Cdkn2a$^{Flox/Flox}$* mice.

(D) Representative H&E staining and IHC of angiosarcoma markers in *aP2-Cre;LSL-Kras^{G12D};Cdkn2a$^{Flox/Flox}$* tumors(n = 6). Scale bars, 50 μm.

See also Figure S4.

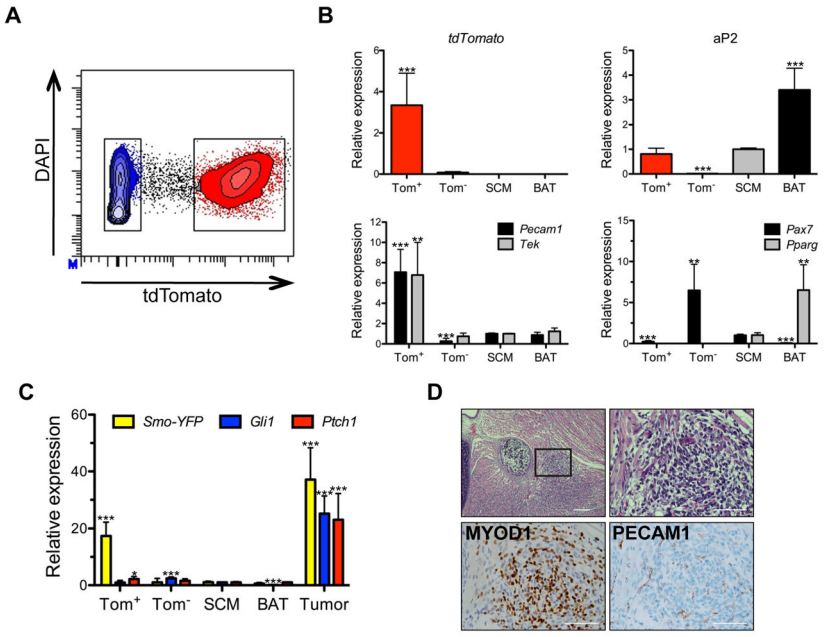

Figure 5. SmoM2 promotes a myogenic fate switch during endothelial cell development

(A) FACS isolation of Tom$^+$ and Tom$^-$ cells from AST SCM.

(B) Gene expression (aP2, *Pecam1, Tek, Pax7* and *Pparg*) of Tom$^+$ and Tom$^-$ cells isolated as in (A) compared to mature SCM and BAT from *Smo*$^{M2/M2}$ mice by real-time PCR. Data shown are normalized to *Actb* expression (tdTomato) or normalized to *Actb* expression and expressed relative to SCM (n = 3, mean ± SEM).

(C) Gene expression of SmoM2-YFP and Shh target genes by real-time PCR in isolated Tom$^+$ and Tom$^-$ cells, mature SCM and BAT from *Smo*$^{M2/M2}$ mice as well as whole tumor from AST mice. Data shown are normalized to *Actb* expression expressed relative to SCM (n = 3, mean ± SEM).

(D) Representative H&E staining and IHC of myogenic marker (MYOD1) and endothelial marker (PECAM1) in sagittal section of E17.5 AST embryo(n = 3). Scale bars, 100 μm (left), 50 μm (right). High magnification of boxed area (right) shown.

*p < 0.05, ** p < 0.01, *** p < 0.001.

See also Figure S5.

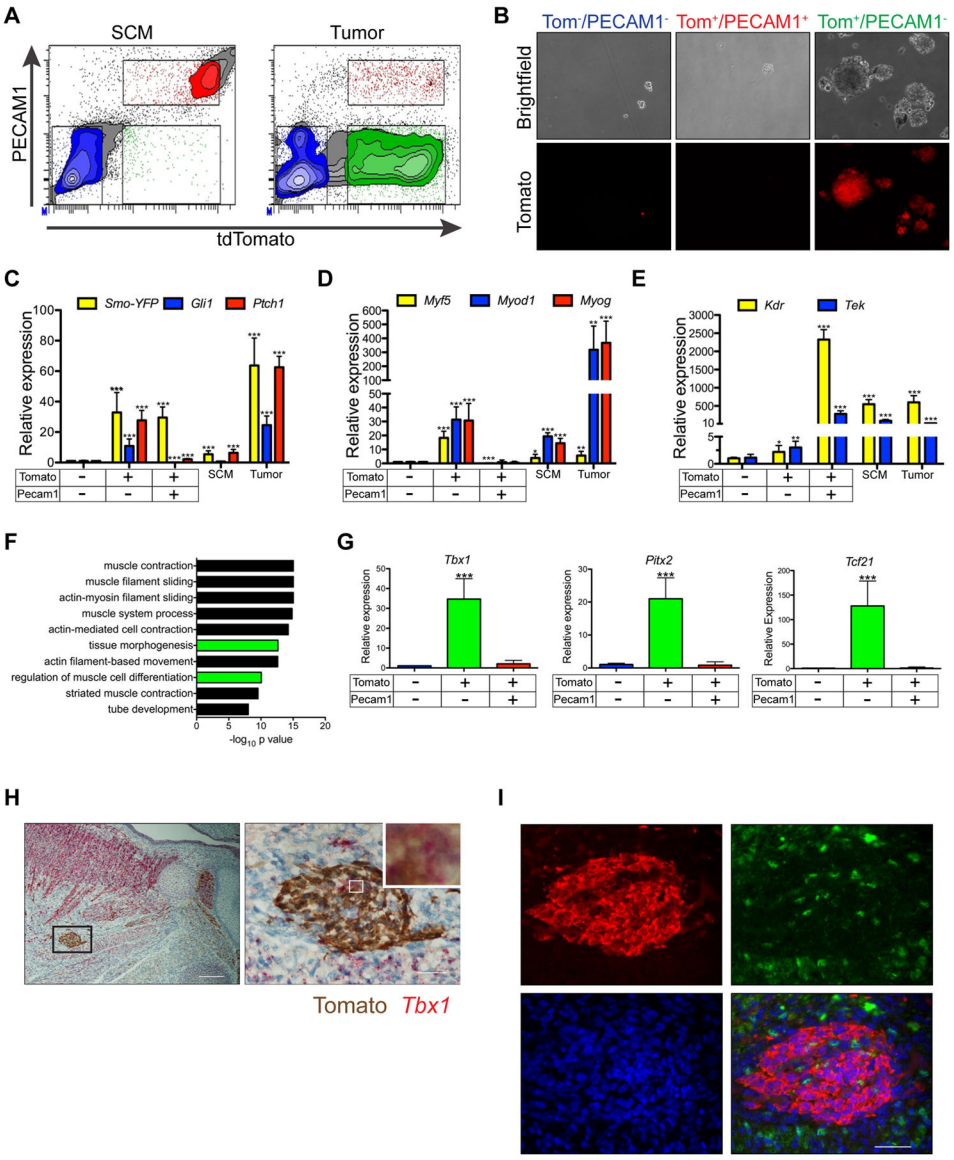

Figure 6. Purified tumor cells retain expression of myogenic specification factors critical for head and neck muscle development

(A) FACS isolation of PECAM1 and Tomato stained cells from AST SCM and tumors.

(B) Sphere formation of tumor cell populations sorted as in (A)(n = 4). Scale bars are 100 μm.

(C–E) Expression of SmoM2-YFP and Shh target genes (C), myogenic markers (D) and endothelial markers (E) in populations isolated as in (A), mature SCM from *Smo*$^{M2/M2}$ mice and whole tumor from AST mice. Data shown are normalized to *Actb* expression and expressed relative to sorted Tom^{-}PECAM1^{-} cells (n = 3, mean ± SEM).

(F) Gene ontology analysis of genes upregulated in Tom^{+}PECAM1^{-} cells versus Tom^{+}PECAM1^{-} cells isolated from AST tumors.

(G) Real-time PCR of myogenic specification factors in cells isolated in (A). Data are analyzed as in (C)(n = 3, mean ± SEM).

(H) Representative dual ISH for *Tbx1* and IHC for Tomato in sagittal section of E15.5 AST embryo. Right panel is enlarged boxed region on left with high magnification inset shown (n = 4). Scale bars, 100 μm (left) and 20 μm (right).

(I) Representative immunostaining for Tomato (red), MYOD1 (green), and DAPI (blue) in sagittal sections of E15.5 AST embryo shown in H. (n = 4). Scale bar, 50 μm.

*$p < 0.05$, ** $p < 0.01$, *** $p < 0.001$.

See also Figure S6 and Tables S1 and S2.

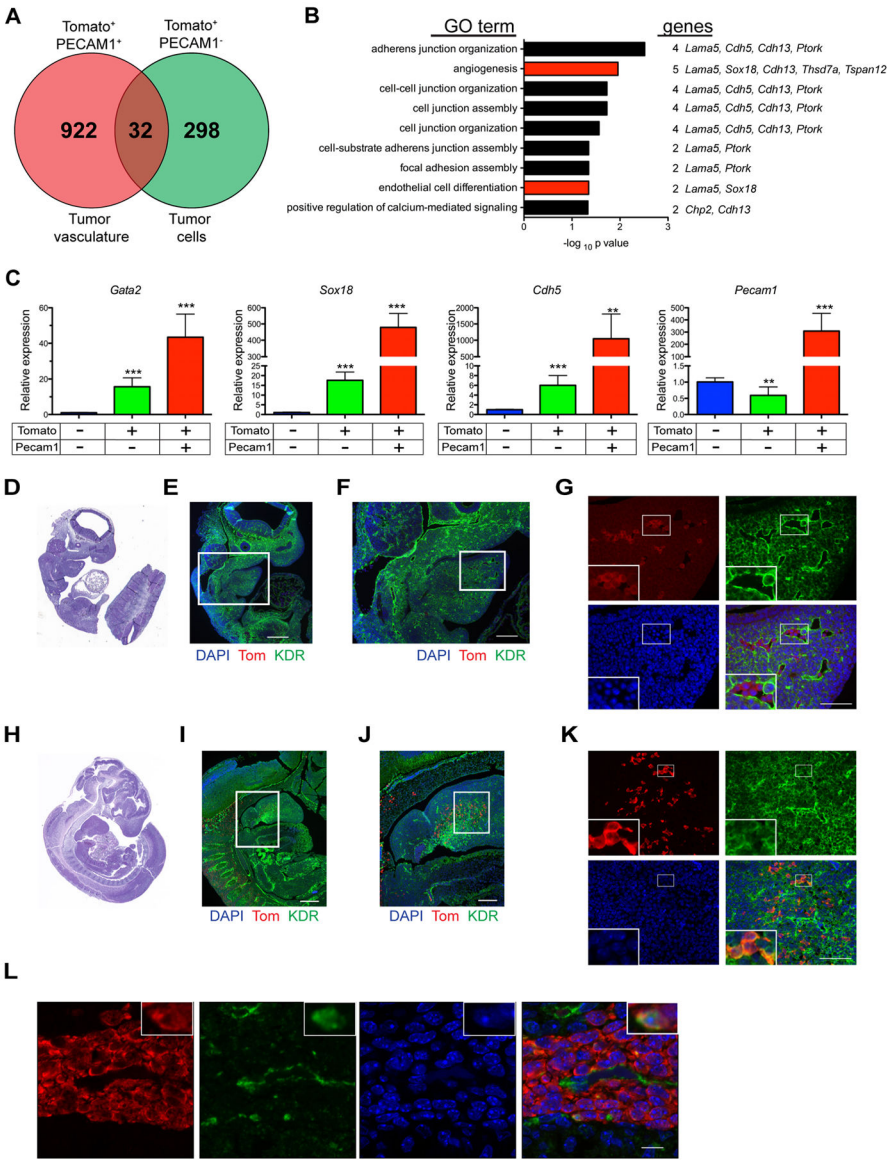

Figure 7. Purified tumor cells and tumor vasculature express common endothelial markers

(A) Venn diagram of genes upregulated in Tom^{+}PECAM1^{-} and Tom^{+}PECAM1^{+} cells compared to Tom^{-}PECAM1^{-} cells isolated from AST tumors.

(B) Gene ontology analysis of 32 overlapping genes from (A).

(C) Gene expression of endothelial genes identified in (A) by real-time PCR. Data shown are normalized to *Actb* expression and expressed relative to sorted Tom^{-}PECAM1^{-} cells (n = 3, mean ± SEM).

(D, E) Representative H&E staining (D) and immunostaining (E) for Tomato (red), KDR (green) and DAPI (blue) on sagittal section of E9.5 AT embryo (n = 2). Scale bars, 250 μm.

(F) Magnification of boxed inset in (E). Scale bars, 100 μm.

(G) Magnification of boxed inset in (F) with high magnification inset in lower left. Scale bars, 50 μm.

(H, I) Representative H&E staining (H) and immunostaining (I) for Tomato (red), KDR (green) and DAPI (blue) on sagittal section of E10.5 AT embryo (n = 4). Scale bars, 250 μm.
(J) Magnification of boxed inset in (I). Scale bars, 100 μm.
(K) Magnification of boxed inset in (J) with high magnification inset in lower left. Scale bars, 50 μm.
(L) Representative immunostaining of Tomato positive proliferations in sagittal sections of E15.5 AST embryo (Figure 6H–I). Tomato (red), KDR (green), DAPI (blue)(n = 4). High magnification insets are shown in upper right. Scale bar, 10 μm.
*$p < 0.05$, ** $p < 0.01$, *** $p < 0.001$.
See also Table S3.

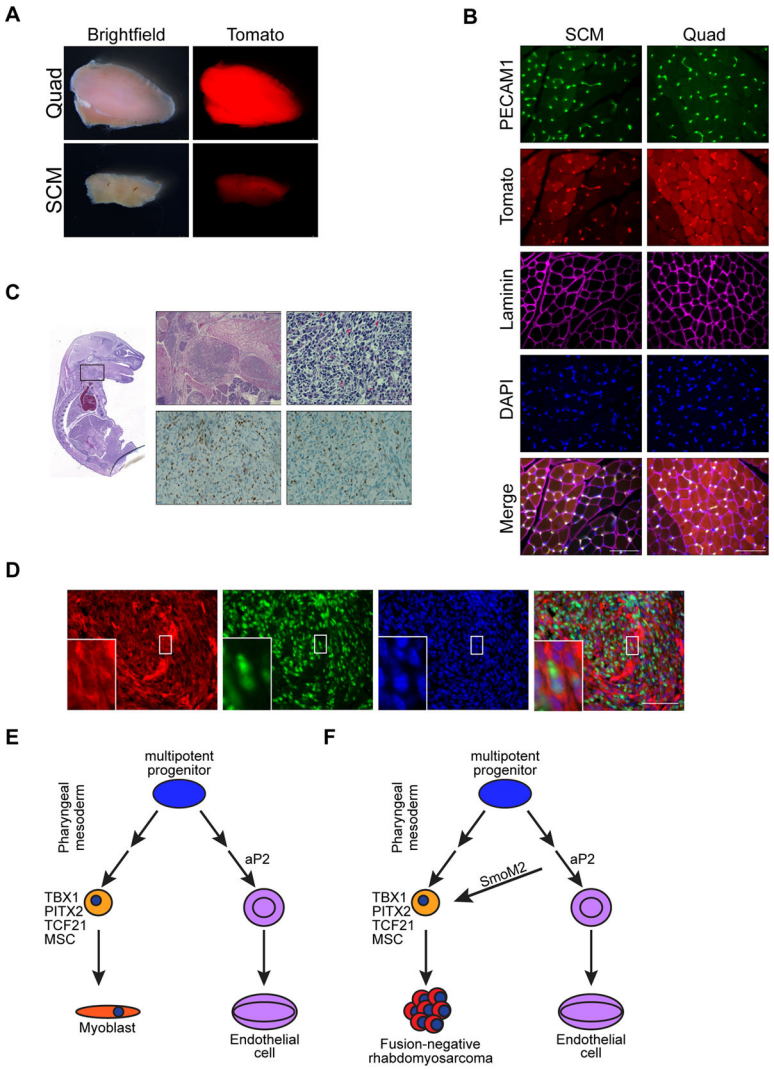

Figure 8. FN-RMS in *Kdr::Cre;Smo$^{M2/+}$* mice

(A) Representative whole mount images of Quad and SCM muscle from *Kdr::Cre;R26-tdTom* mice (n = 3). Scale bar, 1mm.

(B) Representative immunostaining of PECAM1 (green), Tomato (red), LAMININ (magenta) and DAPI (blue) in SCM and quad of *Kdr::Cre;R26-tdTom* mice (n = 3). Scale bars, 50 μm.

(C) Representative sagittal sections of E17.5 *Kdr::Cre;Smo$^{M2/+}$* embryo with H&E staining (top) and IHC for MYOD1 and MYOG (bottom) (n = 4). High magnification of boxed inset shown on top right. Scale bars, 250 μm (top left) and 50 μm (top right and bottom IHC panels).

(D) Representative immunostaining of Tomato (red), MYOD1 (green), DAPI (blue) in tumor from *Kdr::Cre;Smo$^{M2/+}$;R26-tdTom* mice (n = 3). High magnification inset at bottom left of boxed area in center. Scale bar, 50 μm.

(E) Model highlighting KDR expressing multipotent muscle and endothelial cell progenitors in the pharnygeal mesoderm.

(F) Model highlighting rhabdomyosarcomagenesis in *aP2-Cre* expressing cells.

KEY RESOURCES TABLE

REAGENT or RESOURCE	SOURCE	IDENTIFIER
Antibodies		
Rat monoclonal anti-CD34 (Clone RAM 34)	BD Bioscience	Cat# 553731; RRID:AB_395015
Rabbit polyclonal anti-DESMIN	ThermoFisher	Cat # RB-9014; RRID:AB_149771
Rabbit monoclonal anti-ERG	Abcam	Cat # ab133264; RRID:AB_11156852
Mouse monoclonal anti-CK-Oscar (Clone OSCAR)	Covance	Cat #465-01; RRID:AB_2565083
Mouse monoclonal anti-CK-HMV (Clone 34βE12)	DAKO	Cat # M06302
Goat polyclonal anti-KDR	R&D Systems	Cat #AF644; RRID:AB_355500
Rabbit polyclonal anti-Laminin	Sigma	Cat # L9393; RRID:AB_477163
Rat monoclonal anti-Meca32 (Clone Meca 32)	BD Bioscience	Cat #553849; RRID:AB_395086
Mouse monoclonal anti-MHC (Clone MF20)	DSHB	Cat #MF20; RRID:AB_2147781
Mouse monoclonal anti-MYOD1 (Clone 5.8A)	DAKO	Cat #M3512 RRID:AB_2148874
Rabbit monoclonal anti-MYOD1 (Clone EP 212)	Cell Marque	Cat #386R-18
Mouse monoclonal anti-MYOGENIN (Clone F5D)	DAKO	Cat #M3559; RRID:AB_2250893
Mouse monoclonal anti-PAX7	DSHB	Cat #Pax7; RRID:AB_2299243
Rat monoclonal anti-PECAM1 (Clone Mec 13.3)	BD Bioscience	Cat #550274; RRID:AB_393571
Rat monoclonal anti-PECAM1 (Clone SZ31)	Dianova	Cat #Dia 310; RRID:AB_2631039
Rabbit polyclonal anti-S100	DAKO	Cat #Z031129; RRID:AB_2315306
Rabbit polyclonal anti-RFP	Rockland	Cat #600-401-379; RRID:AB_2209751
Goat polyclonal anti-tDTomato	LSBio	Cat #LS-C340696
Rabbit monoclonal anti-VIMENTIN	Novus	Cat #NBP1-40730; RRID:AB_10004971
Hamster monoclonal anti-β1-INTEGRIN (Clone Ha2/5) – FITC conjugated	BD Bioscience	Cat #561796 RRID:AB_10894590
Rat monoclonal anti-CD11b (Clone M1/70) APC conjugate	BD Bioscience	Cat # 553312 RRID:AB_398535
Rat monoclonal anti-CD45 (Clone 30 F11) APC conjugate	BD Bioscience	Cat #561018 RRID:AB_10584326
Rat monoclonal anti-CXCR4 (Clone 2B11/CXCR4) Biotin conjugate	BD Bioscience	Cat #551968 RRID:AB_394307
Rat monoclonal anti-PECAM1 (Clone Mec 13.3) APC conjugate	BD Bioscience	Cat #551262 RRID:AB_398497
Rat monoclonal anti-PECAM1 (Clone Mec 13.3) FITC conjugate	BD Bioscience	Cat #553372 RRID:AB_394818
Rat monoclonal anti-Sca1 (Clone D7) PerCPCy5.5 conjugate	eBioscience	Cat #45-5981-82 RRID:AB_914372
Rat monoclonal anti-TER-119 (Clone TER 119) APC conjugate	BD Bioscience	Cat #557909 RRID:AB_398635
Goat anti-Rat IgG (H+L) Highly Cross-Absorbed Secondary Antibody, Alexa Fluor 488 conjugate	ThermoFisher	Cat #A11006 RRID:AB_2534074
Goat anti-Mouse IgG1 (H+L) Highly Cross-Adsorbed Secondary Antibody, Alexa Fluor 488 conjugate	ThermoFisher	Cat #A21121 RRID:AB_141514
Goat anti-Mouse IgG (H+L) Highly Cross-Absorbed Secondary Antibody, Alexa Fluor 488 conjugate	ThermoFisher	Cat #A11029 RRID:AB_138404
Goat anti-Rabbit IgG (H+L) Highly Cross-Absorbed Secondary Antibody, Alexa Fluor 568 conjugate	ThermoFisher	Cat #A11036 RRID:AB_10563566
Donkey anti-Rabbit IgG (H+L) Highly Cross-Absorbed Secondary Antibody, Alexa Fluor 568 conjugate	ThermoFisher	Cat# A10042 RRID:AB_2534017
Goat anti-Mouse Affinity Purified IgG (H+L) Secondary HRP conjugate	BioRad	Cat# 170-6516 RRID:AB_11125547

REAGENT or RESOURCE	SOURCE	IDENTIFIER
Goat anti-Rat IgG Antibody, HRP conjugate	Millipore	Cat# AP136P RRID:AB_11214444
Donkey anti-Goat IgG (H+L) Highly Cross-Absorbed Secondary Antibody, HRP conjugate	ThermoFisher	Cat# A16005 RRID:AB_2534679
Bacterial and Virus Strains		
Ad5CMV-Cre-eGFP	University of Iowa	VVC-U of Iowa-4
Biological Samples		
Sorted cells from *aP2-Cre;R26-tdTom* mouse sternocleidomastoid	This paper	
Sorted cells from *aP2-Cre;Smo$^{M2/+}$;R26-tdTom* mouse sternocleidomastoid	This paper	
Sorted tumor cells from *aP2-Cre;Smo$^{M2/+}$;R26-tdTom mouse* rhabdomyosarcoma	This paper	
Mononuclear cells from *aP2-Cre;Smo$^{M2/+}$;R26-tdTom* mouse sternocleidomastoid	This paper	
Mononuclear cells from *aP2-Cre;Smo$^{M2/+}$;R26-tdTom* mouse sternocleidomastoid	This paper	
aP2-Cre;R26-LacZ hindlimb muscle myoblast	This paper	
Smo$^{M2/M2}$ mouse sternocleidomastoid	This paper	
Smo$^{M2/M2}$ mouse brown adipose tissue	This paper	
Rhabdomyosarcoma from *aP2-Cre;Smo$^{M2/+}$;R26-tdTom* mice	This paper	
Chemicals, Peptides, and Recombinant Proteins		
Collagenase B	Roche	Cat # 11088831001
Dispase II	Roche	Cat # 4942078001
Liberase DL	Roche	Cat # 05401160001
bFGF	R&D Systems	Cat # 233-FB-025
EGF	R&D Systems	Cat # 23626
B27 Supplement	Gibco	Cat # 17504-44
Critical Commercial Assays		
TSA plus Fluorescein System	Perkin-Elmer	Cat# 741E001KT
Vectashield Hardset mounting medium with DAPI	Vector Laboratories	Cat# H1500
miRNeasy micro kit	Qiagen	Cat# 217084
miRNeasy mini kit	Qiagen	Cat# 217004
Superscript Reverse Transcriptase	ThermoFisher	Cat# 18080051
Fast SYBR Green Master Mix	ThermoFisher	Cat# 4385610
TaqMan Fast Advanced Master Mix	ThermoFisher	Cat# 4444964
Ovation Pico WTA system V2	Nugen	Cat# 3302
Mouse gene 2.0 ST microarray	Affymetrix	Cat#902118
RNAscope 2.5 VS-probe-Mm-Tbx1	ACD	Cat#481919
Deposited Data		
Microarray data	This Paper	GSE 98059
Microarray data – *aP2-Cre;SmoM2 RMS, MyoG-Cre;SmoM2 RMS*	(Hatley et al., 2012)	GSE 40359

REAGENT or RESOURCE	SOURCE	IDENTIFIER
Microarray data – C57/Bl6 sternocleidomastoid muscle	(Hanna et al., 2017)	GSE 85834
Microarray data – microvascular endothelial cells	(Nolan et al., 2013)	GSE 47067
Microarray data – brown and white adipose	(Seale et al., 2007)	GSE 8044
Microarray data – satellite cells and PWI expressing interstitial cells	(Pannerec et al., 2013)	GSE 40523
Experimental Models: Cell Lines		
Experimental Models: Organisms/Strains		
Mouse: *B6.SJL-Tg(aP2-Cre)Jmg*		
Mouse: *B6;FVB-Tg(Adipoq-Cre)1Evdr/J*	Jackson Laboratories (Eguchi et al., 2011)	Cat # 10803 RRID:IMSR_JAX:010803
Mouse: *B6.FVB-Tg(Ucp1-Cre)1Evdr/J*	Jackson Laboratories (Kong et al., 2014)	Cat # 24670 RRID:IMSR_JAX:024670
Mouse: *B6.Cg-Tg(Fabp4-Cre)1Rev/J*	Jackson Laboratories (He et al., 2003)	Cat # 5069 RRID:IMSR_JAX:005069
Mouse: $Kdr^{tm1(Cre)Sato}/J$	Jackson Laboratories (Motoike et al., 2003)	Cat # 018976 RRID:IMSR_JAX:018976
Mouse: $B6.129(Cg)\text{-}Gt(ROSA)26Sor^{tm4(ACTB\text{-}tdTomato,\text{-}EGFP)Luo}/J$	Jackson Laboratories (Muzumdar et al., 2007)	Cat # 7676 RRID:IMSR_JAX:007676
Mouse: $B6.Cg\text{-}Gt(ROSA)26Sor^{tm14(CAG\text{-}tdTomato)Hze}/J$	Jackson Laboratories (Madisen et al., 2010)	Cat # 7914 RRID:IMSR_JAX:007914
Mouse: $B6.129S4\text{-}Gt(ROSA)26Sor^{tm1Sor}/J$	Jackson Laboratories (Soriano, 1999)	Cat # 3474 RRID:IMSR_JAX:003474
Mouse: $Gt(ROSA)26Sor^{tm1(Smo/EYFP)Amc}/J$	Jackson Laboratories (Mao et al., 2006)	Cat # 5130 RRID:IMSR_JAX:005130
Mouse: $B6.129S4\text{-}Kras^{tm4Tyj}/J$	Jackson Laboratories (Jackson et al., 2001)	Cat # 8179 RID:IMSR_JAX:008179
Mouse: $Cdkn2a^{flox/flox}$	(Aguirre et al., 2003)	
Oligonucleotides		
SYBR primers for real-time PCR – see Table S6		
Taqman FAM Probe – *Gli1*	ThermoFisher	Cat # Mm00494654_m1
Taqman FAM Probe – *MyoG*	ThermoFisher	Cat # Mm00446195_g1
Taqman FAM Probe – *Msc*	ThermoFisher	Cat # Mm00447887_m1
Taqman FAM Probe – *Pax3*	ThermoFisher	Cat # Mm00435491_m1
Taqman FAM Probe – *Pitx2*	ThermoFisher	Cat # Mm01316994_m1
Taqman FAM Probe – *Tbx1*	ThermoFisher	Cat # Mm00448949_m1
Taqman FAM Probe – *Lgr4*	ThermoFisher	Cat # Mm00554385_m1
Software and Algorithms		
Nikon Elements Basic Research v4.13	Nikon Instruments Inc	
Leica Application Suite X	Leica Microsystems	
FACSdiva v8.0.1	BD Biosystems	
Graphpad Prism 6	Graphpad software	

REAGENT or RESOURCE	SOURCE	IDENTIFIER
Image J v1.50	NIH	
STATA/MP 14.2	StataCorp	
Partek Genome Suite 6.6	Partek	
Enrichr gene enrichment analysis tool	(Chen et al., 2013b; Kuleshov et al., 2016)	
Adobe Photoshop CS5.1	Adobe Software	
Adobe Illustrator CS5.1	Adobe Software	
Other		